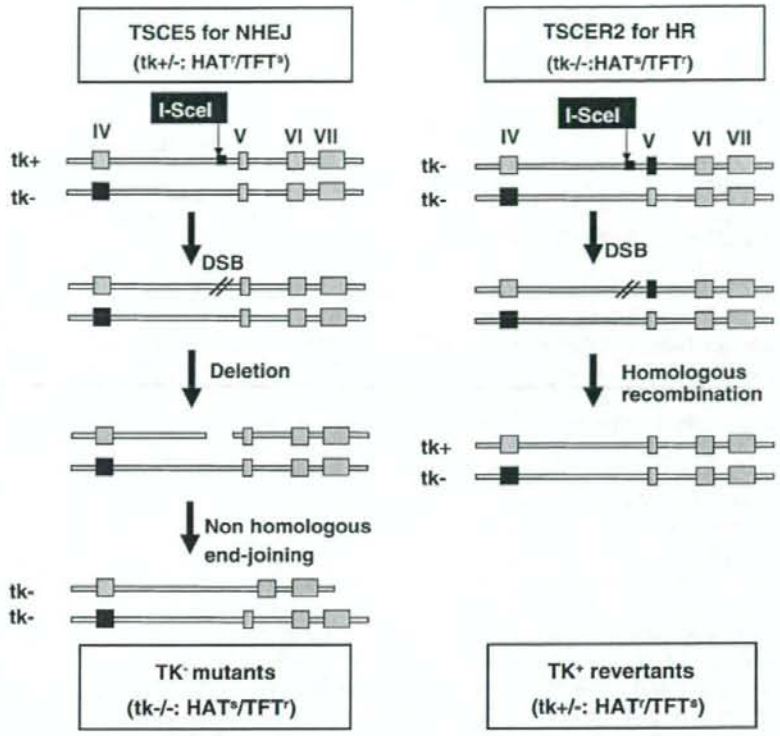

Fig. 1 Strategy of DSB repair assays for I-SceI double strand breaks. The two constructed cell lines—the original TSCE5 line containing the I-SceI recognition insert and its derived compound heterozygote TSCER2—are shown together with the selectable phenotypes generated by repair of double strand breaks (DSBs) through non-homologous end-joining (NHEJ) in TSCE5 cells or homologous repair (HR) in TSCER2 cells (see text)

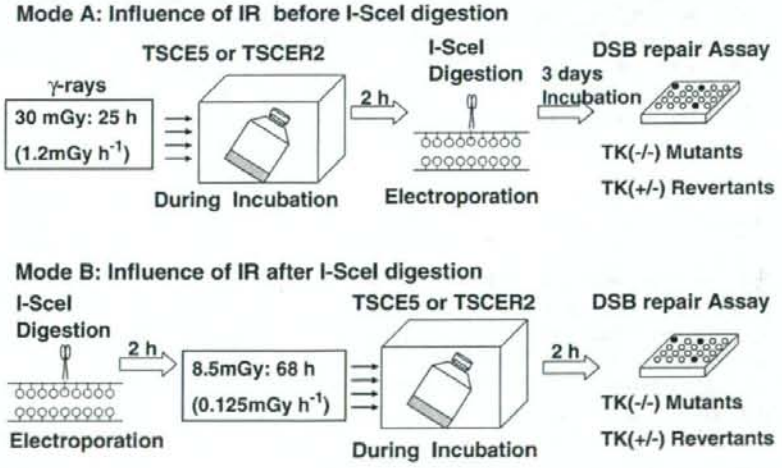

Fig. 2 Experimental scheme of radiation exposure and I-SceI expression. In mode A, cells were exposed to low-dose, low-dose-rate γ-irradiation and then transfected with the I-SceI vector by electroporation (see text). In *mode B* cells were transfected with the I-SceI vector and then exposed to γ-irradiation at a much lower dose and dose-rate (see text)

Determination of TK^- mutants and TK^+ revertants

In mode A, immediately after transfection the cells were suspended in 50 ml of fresh RPMI1640 medium, incubated for 3 days, and then seeded into 96-microwell plates. In mode B, the cell seeding was done at 2 h after the irradiation/incubation following the I-SceI digestion as described above. TSCE5 cells were seeded at 100 cells per well and incubated in the presence of 2.0 μg ml^{-1} trifluorothymidine (TFT) for the detection of TK-deficient

mutants. TSCER2 cells were seeded at 2,000 cells per well in the presence of HAT (200 μM hypoxanthine, 0.1 μM aminopterin, 17.5 μM thymidine) for the detection of TK-proficient revertants.

Results

TK mutant frequency after γ-irradiation

Table 1a shows frequencies of TK^- mutants in TSCE5 cells not expressing I-SceI without irradiation (control) and after exposure to 30 mGy γ-irradiation at 1.2 mGy h^{-1} (mode A). The mean TK^- mutant frequency (MF) values were found to be 2.7×10^{-6} and 4.7×10^{-6} for control and γ-irradiated sample, respectively, and both the level of MFs and the increase caused by γ-irradiation were consistent with those of a previous investigation [3]. Table 2a shows TK^- mutant frequency in unirradiated control TSCE5 cells and cells that were exposed to 8.5 mGy γ-irradiation at 0.125 mGy h^{-1} (mode B). The mean TK^- MF values for un- and γ-irradiated cells in the mode B experiment (3.0×10^{-6} and 2.1×10^{-6}, respectively) were very similar to values obtained after the 12 mGy exposure (at the same dose-rate as in mode B), namely 3.2×10^{-6} and 2.0×10^{-6} for un- and γ-irradiated sample, respectively. These results suggest that the lower doses (8.5 and 12 mGy) delivered at a lower does rate (0.125 mGy h^{-1}) did not enhance the TK^- mutant frequency but rather reduced it. We did not determine the frequency of TK^+ revertants for unirradiated control and γ-irradiated TSCER2 cells because we expected those frequencies to be too low for us to accurately estimate the effect of IR exposure. In fact, the spontaneous revertant frequency (RF) in TSCER2 is in the range of 10^{-8} [4, 5].

Effect of radiation exposure prior to I-SceI transfection on DSB repair (mode A)

In the mode A experiment, the low-dose, low-dose-rate γ-irradiation was performed prior to transfection with the I-SceI vector to estimate the influence of pre-IR exposure on repair of I-SceI introduced DSB. We calculated the relative TK^- mutant frequency MF_{rel} = (MF (γ-rays + I-SceI)/MF (I-SceI)) for each experiment because the transfection efficiencies varied. The mean MF_{rel} in TSCE5 cells exposed to IR prior to transfection was 1.0 (Table 1a), indicating that irradiation had no effect on NHEJ repair of I-SceI-induced DSBs. The relative TK^+ revertant frequency, RF_{rel} in TSCER2 cells was determined in an analogous manner. Exposure to irradiation prior to transfection consistently enhanced RF_{rel}, and the mean RF_{rel} was 1.5 (Table 1b), indicating that irradiation enhanced the HR repair of DSBs by 50%. This 50% increase was found to be statistically significant by *t*-test ($P = 0.021$, if taken as paired data).

Table 1 Effect on DSB repair of exposure to 30 mGy IR at 1.2 mGy h^{-1} prior to transfection with I-SceI expression vector (mode A)

a) NHEJ efficiency in TSCE5 cells

Exp.	TK^- Mutant Frequency, MF ($\times 10^{-6}$)				Effect of IR (MF_{rel}[a])
	Control	γ-rays	I-SceI	γ-rays + I-SceI	
1	3.5	6.1	8,600	8,500	0.99
2	1.8	3.2	2,900	3,200	1.1
Mean	2.7	4.7	5,800	5,900	1.0 ($P = 0.82$)[c]

b) HR efficiency in TSCER2 cells

Exp.	TK^+ Revertant Frequency, RF ($\times 10^{-6}$)				Effect of IR (RF_{rel}[b])
	Control	γ-rays	I-SceI	γ-rays + I-SceI	
1	–	–	90	114	1.3
2	–	–	62	96	1.5
3	–	–	25	45	1.8
Mean	–	–	59	85	1.5 ($P = 0.021$)[c]

[a] MF_{rel} was calculated as MF (γ-rays + I-SceI)/MF (I-SceI)

[b] RF_{rel} was calculated as RF (γ-rays + I-SceI)/RF (I-SceI)

[c] Assuming that they were paired data, *P* value was calculated by *t*-test

Table 2 Effect on DSB repair of exposure to 8.5 mGy IR at 0.125 mGy h^{-1} following transfection with I-SceI expression vector (mode B)

a) NHEJ efficiency in TSCE5 cells

Exp.	TK^- Mutant Frequency, MF ($\times 10^{-6}$)				Effect of IR (MF_{rel}[a])
	Control	γ-rays	I-SceI	γ-rays + I-SceI	
1	2.8	1.3	3,400	4,500	1.3
2	3.1	2.8	12,000	17,000	1.4
3	–	–	11,000	11,000	1.0
Mean	3.0	2.1	8,800	10,800	1.2 ($P = 0.12$)[c]

b) HR efficiency in TSCER2 cells

Exp.	TK^+ Revertant Frequency, RF ($\times 10^{-6}$)				Effect of IR (RF_{rel}[b])
	Control	γ-rays	I-SceI	γ-rays + I-SceI	
1	–	–	82	160	2.0
2	–	–	160	270	1.7
3	–	–	110	190	1.7
Mean	–	–	120	210	1.8 ($P = 0.0013$)[c]

[a] MF_{rel} was calculated as MF (γ-rays + I-SceI)/MF (I-SceI)

[b] RF_{rel} was calculated as RF (γ-rays + I-SceI)/RF (I-SceI)

[c] Assuming that they were paired data, *P* value was calculated by *t*-test

Effect of radiation exposure after I-SceI transfection on DSB repair (Mode B)

In the mode B experiment, the γ-irradiation was performed after transfection with the I-SceI vector to estimate the post-IR exposure effects on DSB repair. The mean MF_{rel} in TSCE5 cells exposed to IR following transfection was 1.2 (Table 2a) and the difference between unirradiated and irradiated cells was not statistically significant, indicating that post-transfection γ-irradiation had hardly any effect on NHEJ repair of DSBs. The mean RF_{rel} in TSCER2 cells under the same conditions, however, was 1.8 (Table 2b), indicating that exposure to γ-irradiation following transfection with I-SceI enhanced the HR repair of DSBs by 80%. This 80% increase was also found to be statistically significant by *t*-test ($P = 0.0013$, if taken as paired data).

Discussion

The efficiency of transfection using the amaxa nucleofection system was estimated to be about 40-fold higher than that using BioRad electroporation system, and this higher efficiency enabled us to more accurately estimate the repair of a single DSB at the specific I-SceI recognition site. As in our previous studies [4, 5], we observed that the frequencies of TK^+ revertants after the I-SceI vector transfection were lower than those of TK^- mutants. That finding seems to be consistent with the notion that NHEJ is the major repair pathway in mammalian cells [9]. Because our I-SceI system does not cover all NHEJ and HR events, it is however difficult to estimate the extent of DSB repair by HR. For example, our system does not cover sister-chromatid HR, which is probably the major HR pathway in mammalian cells. Small gene conversion events, not expanding to the exon 5 region, also cannot be detected by this system. Furthermore, there might be unkown factors, specific to this I-SceI site, which reduce the occurrences of the gene conversion type of events. Although the I-SceI system might over-estimate the repair efficiency of NHEJ compared with HR, it is a good model for elucidating the DSB repair associated with low-dose IR exposure.

Although transfection efficiencies varied from experiment to experiment, the relative TK^- mutant frequency and TK^+ revertant frequency were sufficient for evaluating the influence of IR on DSB repair. Both modes (A and B) of delivering low-dose, low dose-rate γ-irradiation were found to hardly influence NHEJ at the I-SceI site. Since an adaptive mutagenic response, a reduction of TK^- mutation frequency, was observed in TK6 cells exposed to X-rays (5 cGy of priming dose and 2 Gy of challenge dose) [10], we also measured DSB repair in cells in which the challenging X-ray exposure was replaced by I-SceI digestion. In those measurements, similarly, NHEJ was barely influenced by the priming X-ray radiation (unpublished data), suggesting that an acute low-dose IR exposure also might provide the same tendency of "no influence" as that observed with the low-dose, low-dose-rate γ-irradiation. In contrast to NHEJ, both modes of γ-irradiation in the present experiments were found to considerably enhance HR at the I-SceI sites. This enhanced HR was not due to radiation-induced S/G2 arrest, because the low-dose IR did not affect the cell cycle (data not shown). Similar results were obtained when using a priming X-radiation (5 cGy; unpublished data).

The above similarities suggest that the enhancement of HR repair observed in the present study is a manifestation of an adaptive response where the low-dose, low-dose-rate γ-irradiation was the priming exposure. The inefficient effect of γ-irradiation on NHEJ does not seem to be consistent with a higher efficiency of DSB repair in radioadapted cells [11], as was shown by the reduction of genetic alterations at the chromosome level [12–14]. Since IR-induced DSBs were the major targets for adaptation in those studies, their DSBs might differ in some way from the I-SceI-induced DSBs we report on here. In other words, the fate of site-specific I-SceI breaks might reflect repair of spontaneous DSBs more faithfully than that of DSBs induced directly by relatively high dose exposure. At the present stage, it is very difficult to speculate plausible mechanisms responsible for the apparent adaptive response of DSB repair. We believe that the characteristics of I-SceI breaks and their continuous generation after the transfection are related to the observed repair characteristics. The enhanced repair by HR upon low-dose, low-dose-rate γ-irradiation is obviously not due to an enhanced cleavage of the I-SceI site after irradiation, since we have not observed such enhanced repair by NHEJ.

It remains to be tested whether NHEJ is really not enhanced by low-dose, low-dose-rate IR or whether it apparently remained stable because of limitations of the methodology. Recently, the fates of I-SceI breaks located in TSCE5 cells were determined in randomly isolated clones using non-phenotypic selection [5]. About 97% of the clones showed perfect rejoining, and deletions corresponding to the events detectable by the present selection method (i.e. large enough to affect the adjacent exon) were found in only 0.54% of the clones. Thus, if perfect NHEJ events or small deletion events were enhanced by low-dose, low-dose-rate γ-irradiation, we would not detect them by the present methodology.

In addition, the mechanisms responsible for HR repair, which is active in S/G2 phase cells, remains to be elucidated. In our previous studies using genetic analyses, we observed small homozygous LOH events in primed cells in the X-ray plus X-ray radioadaptive experiment mentioned

above [10]. We observed the same pattern of LOH mutants after low-dose, low-dose-rate γ-ray exposures [3], although the frequency was low. These results can be explained by the enhanced contribution of HR observed in the I-SceI digestion system, because this system could recover the non-crossing over gene conversion events very efficiently among the TK^+ revertants. In near future we need to elucidate HR pathway leading to gene conversion, where a central core of protein, most likely the RecA homolog RAD51, plays a key role [15].

DSBs arise from endogenous sources including reactive oxygen species generated during cellular metabolisms. The DSB generation process mediated by reactive oxygen is suggested to be also involved in the indirect effects of the ionizing radiation exposure. As already described, the site-specific I-SceI break in our system can be considered as a good model for endogeneous DSBs. Thus, enhanced HR repair activity induced by low-dose, low-dose-rate IR, might be regarded as defense machinery against DNA damage, whether occurring spontaneously and/or after low-dose, low-dose rate IR. At present, we are making an effort to apply the I-SceI digestion system for estimating DSB repair in bystander cells.

Acknowledgments This study was partially supported by the Budget for Nuclear Research of the Ministry of Education, Culture, Sports, Science and Technology, and was reviewed by the Atomic Energy Commission of Japan. We thank Dr. Miriam Bloom (SciWrite Biomedical Writing & Editing Services) for professional editing.

References

1. Morimoto S, Kato T, Honma M, Hayashi M, Hanaoka F, Yatagai F (2002) Detection of genetic alterations induced by low-dose X rays: analysis of loss of heterozygosity for *TK* mutation in human lymphoblastoid cells. Radiat Res 157:533–538
2. Morimoto S, Honma M, Yatagai F (2002) Sensitive detection of LOH events in a human cell line after C-ion beam exposure. J Radiat Res 43(Suppl):S163–S167
3. Umebayashi Y, Honma M, Suzuki M, Suzuki H, Shimazu T, Ishioka N, Iwaki M, Yatagai F (2006) Mutation induction in cultured human cells after low-dose and low-dose-rate γ-ray irradiation: detection by LOH analysis. J Radiat Res 48:7–11
4. Honma M, Izumi M, Sakuraba M, Tadokoro S, Sakamoto H, Wang W, Yatagai F, Hayashi M (2003) Deletion, rearrangement, and gene conversion; genetic consequences of chromosomal double-strand breaks in human cells. Environ Mol Mutagen 42:288–298
5. Honma M, Sakuraba M, Koizumi T, Takashima T, Sakamoto H, Hayashi M (2007) Non-homologous end-joining for repairing I-SceI induced DNA double strand breaks in human cells. DNA Repair 6:781–788
6. Jackson SP (2002) Sensing and repairing DNA double-strand breaks. Carcinogenesis 23:687–696
7. Valerie K, Povirk LF (2003) Regulation and mechanisms of mammalian double-strand break repair. Oncogene 22:5792–5812
8. Jeggo PA (1998) DNA breakage and repair. Adv Genet 38:185–282
9. Pastwa E, Blasiak J (2003) Non-homologous end-joining. Acta Biochim Pol 50:891–908
10. Yatagai F, Umebayashi Y, Honma M, Sugasawa K, Takayama Y, Hanaoka F (2007) Mutagenic radioadaptation in a human lymphoblastoid cell line. Mutat Res 638:48–55
11. Ikushima T, Aritomi H, Morisita J (1996) Radioadaptive response: efficient repair of radiation-induced DNA damage in adapted cells. Mutat Res 358:193–198
12. Rigaud O, Papadopoulo D, Moustacchi E (1993) Decreased deletion mutation in radioadapted human lymphoblast. Radiat Res 133:94–101
13. Azzam EI, Raaphorst GP, Mitchel RE (1994) Radiation-induced adaptive response for protection against micronucleus formation and neoplastic transformation in C3H 10T1/2 mouse embryo cells. Radiat Res 138:S28–S31
14. Ueno AM, Vannais DB, Gustafson SL, Wong JC, Waldren CA (1996) A low adaptive dose of gamma-rays reduced the number and altered the spectrum of S1 mutants in human hamster hybrid cells. Mutat Res 358:161–169
15. Li X, Heyer W-D (2008) Homologous recopmbination in DNA repair and DNA damage tolerance. Cell Res 18:99–113

DNA REPAIR 7 (2008) 663–669

available at www.sciencedirect.com

ScienceDirect

journal homepage: www.elsevier.com/locate/dnarepair

DNA Repair

Brief report

Mutagenesis of uracil-DNA glycosylase deficient mutants of the extremely thermophilic eubacterium *Thermus thermophilus*

*Tomoya Sakai, Shin-ichi Tokishita, Kayo Mochizuki, Ayako Motomiya, Hideo Yamagata, Toshihiro Ohta**

School of Life Sciences, Tokyo University of Pharmacy and Life Sciences, 1432-1 Horinouchi, Hachioji, Tokyo 192-0392, Japan

ARTICLE INFO

Article history:
Received 20 September 2007
Received in revised form
7 January 2008
Accepted 14 January 2008

Keywords:
Uracil-DNA glycosylase
Thermus thermophilus
Mutator
Bgl assay

ABSTRACT

Thermus thermophilus is an extremely thermophilic, aerobic, and gram-negative eubacterium that grows optimally at 70–75 °C, pH 7.5. In extremely high temperature environment, DNA damages in cells occur at a much higher frequency in thermophiles than mesophiles such as *E. coli*. When temperature rises, the deamination of cytosine residues in double-strand DNA is expected to increase greatly. *T. thermophilus* HB27 has two putative uracil-DNA glycosylase genes (*udgA* and *udgB*). Expression level of *udgA* gene was 2–3 times higher than that of *udgB* at 70, 74, and 78 °C when it was monitored by β-glucosidase reporter assay. We developed $hisD_{3110}$, $hisD_{3113}$, $hisD_{3115}$, and $hisD_{174}$ marker allele that can specifically detect G:C → A:T, C:G → A:T, T:A → A:T, and A:T → G:C base-substitutions, respectively, by His$^+$ reverse mutations. We then disrupted *udgA* and *udgB* by thermostable kanamycin-resistant gene (*htk*) or *pyrE* gene insertion in each *hisD* background, and their spontaneous His$^+$ reversion frequencies were compared. A *udgA,B* double mutant showed a pronounced increase in G:C → A:T reversion frequency compared with each single *udg* mutant, *udgA* or *udgB*. Estimated mutation rates of the *udgA,B* mutant cultured at 60, 70, and 78 °C were about 2, 12, and 117 His$^+$/10^8/generation, respectively. At 70 °C culture, increased ratio of the mutation rate compared with the *udg*$^+$ strain was 12-fold in *udgA*, 3-fold in *udgB*, and 56-fold in *udgA,B* mutant. On the other hand, no difference was observed in other mutations of C:G → A:T, T:A → A:T, and A:T → G:C between *udgA,B* double mutant and the parent *udg*$^+$ strain. The present results indicated that gene products of *udgB* as well as *udgA* functioned in vivo to remove uracil in DNA and prevent G:C → A:T transition mutations.

1. Introduction

Thermus thermophilus HB27, isolated from a Japanese thermal spa, is an extremely thermophilic eubacterium that grows at 55–82 °C [1]. It is a nonsporulating, gram-negative, aerobic, obligate heterotroph that grows optimally at 70–75 °C and pH 7.5. Because of the rapid growth rate of *T. thermophilus* and the ease of purifying its proteins, its thermostable enzymes have been extensively studied in vitro, including in a structural genomics project [2]. The genome of the strain HB27

* *Corresponding author*. Tel.: +81 42 676 7093; fax: +81 42 676 7081.
E-mail address: ohta@ls.toyaku.ac.jp (T. Ohta).
1568-7864/$ – see front matter © 2008 Elsevier B.V. All rights reserved.
doi:10.1016/j.dnarep.2008.01.006

has been sequenced [3] and consists of about 2200 putative genes divided between a 1.89 Mbp chromosome and a 0.23 Mbp megaplasmid (pTT27). *T. thermophilus* shows natural transformation competence throughout its growth phase with efficiency on the order of 10^4 transformants/μg DNA [4]. Although available antibiotic resistance genes at 70 °C are limited, a host–vector system was developed using the cryptic plasmid pTT8 (copy number: 8/cells) with a thermostable kanamycin-resistant *htk* gene [5]. On the other hand, a chemically defined medium for HB27 has been developed [6]. It provides a genetic method using auxotroph mutants.

Our major interest is DNA repair systems that function in extremely high temperature environments and the mechanisms of mutagenesis in *T. thermophilus*, because we would expect endogenous DNA damage such as deamination, depurination, methylation, oxidation, and single strand breaks to occur at a much higher frequency in thermophiles than in mesophiles. The spontaneous hydrolytic deamination of cytosine to uracil occurs frequently in the intracellular environment. A mismatched base pair G:U resulting from cytosine deamination generates an A:U base pair after replication. Subsequent replication of an A:U base pair should result in G:C→A:T transition mutation [7,8]. To prevent the occurrence of mutations by uracil in DNA, a base excision repair pathway has an important role [9]. Uracil-DNA glycosylase (UDG) catalyzes the first step in the repair pathway for uracil-containing DNA. The enzyme releases uracil from DNA by hydrolyzing the bond between the base and a deoxyribose [10]. Based on the amino acid sequences similarity and differences in substrate specificity, UDGs are classified into five families [9,11]. Family 1 UDGs (Ung family) excise uracil base from single-stranded DNA and double-stranded DNA. *E. coli* Ung is the representative of this family. Family 1 UDGs are found in many organisms including bacteria, yeast, mammalian cells, and plant cells, but not in archaea and insects. Family 2 UDGs (Mug/TDG family) consist of bacterial mismatch-specific uracil-DNA glycosylases (Mug) [12] and eukaryotic thymine-DNA glycosylases (TDG) [13,14]. They remove 3, N^4-ethenocytosine as well as uracil when mispaired with guanine. It has been reported that *E. coli* mug mutant showed no effect on G:C→A:T mutations [15]. Therefore, the principal role of family 2 UDGs may be the removal of 3, N^4-ethenocytosine. Family 3 UDGs (SMUG family) are single-strand-specific monofunctional uracil-DNA glycosylases (SMUG) and are identified in vertebrates and insects. They act on uracil and 5-hydroxymethyluracil in DNA [16]. Quite recently a bacterial SMUG ortholog has been reported in *Geobacter metallireducens* [17]. Family 4 UDGs (TmUDG) are thermostable UDG family found in thermophilic archaea and bacterial species. *Thermotoga maritima* UDG (TmUDG) is the representative of this family [18]. Family 4 enzymes from hyperthermophile archaea *Archaeoglobus fulgidus* [19] and *Pyrobaculum aerophilum* [20] are also characterized. They remove uracil from duplex DNA and single-stranded DNA containing uracil. Family 5 UDGs (UDG-b family) are found only in hyperthermophilic archaeon *P. aerophilum* [21] and eubacterium *T. thermophilus* [22]. They act on uracil in duplex DNA. PaUDG also catalyzes the removal of hypoxanthine, a product of adenine deamination. This enzyme, therefore, may play an important role against deamination of both cytosine and adenine. In addition to the above five UDG families, a novel UDG has been identified from hyperthermophilic archaeon *Methanococcus jannaschii* [23]. The MjUDG catalyzes the excision of 8-hydroxyguanine as well as uracil from DNA.

T. thermophilus HB27 has two putative UDG genes, *udgA* (TTC0366) and *udgB* (TTC0784) [22]. The former belongs to the family 4 UDGs and the latter is the family 5 UDGs. Since there is no report on isolation and characterization of *udg*-deficient mutants of *T. thermophilus*, little is known about the function and complementation of the two genes in vivo at growing temperature. We first investigated expression level of the *udgA* and *udgB* genes at different temperature by a newly developed β-glucosidase (Bgl) reporter assay. We demonstrate the constitutive expression of both the genes. Then, we developed a set of *hisD* reverse mutation assay system to determine the mutation spectrum and used it to investigate mutator phenotype of *udg* mutants. We report here the evidence that gene products of *udgB* as well as *udgA* functioned in vivo to prevent G:C→A:T transition mutations.

2. Materials and methods

2.1. *Bacterial strains, culture media, and chemicals*

Table 1 shows the strains of *T. thermophilus* used in this study. Bacteria were cultured in PY medium (0.8% polypeptone, 0.4% Difco yeast extract, 0.2% NaCl, 0.35 mM $CaCl_2$, and 0.4 mM $MgCl_2$) at 70 °C with shaking. MSG minimal medium (pH 7.5) consisted of 2% sucrose, 2% sodium glutamate, 0.2% NaCl, 0.05% $(NH_4)_2SO_4$, 0.05% K_2HPO_4, 0.025% KH_2PO_4, 88 μg/ml $CaCl_2{\cdot}2H_2O$, 35 μg/ml $MgCl_2{\cdot}6H_2O$, 1.2 μg/ml $Na_2MoO_4{\cdot}2H_2O$, 0.5 μg/ml $MnCl_2{\cdot}4H_2O$, 0.1 μg/ml $VOSO_4{\cdot}nH_2O$, 0.06 μg/ml $ZnSO_4{\cdot}7H_2O$, 0.08 μg/ml $CoCl_2{\cdot}6H_2O$, 0.015 μg/ml $CuSO_4{\cdot}5H_2O$, 0.002 μg/ml $NiCl_2{\cdot}6H_2O$, 6.7 μg/ml $FeSO_4{\cdot}7H_2O$, 0.1 μg/ml biotin, and 1 μg/ml thiamine. Medium was solidified with 1.5% agar for culture at 70 °C or 1.5% gellan gum for culture at 74 °C. Top agar contained 0.6% agar without NaCl. *Escherichia coli* strain XL1-Blue MRF' and vector plasmids pCR4-TOPO (Invitrogen Japan K.K., Tokyo) were used for plasmid construction. Gellan gum, 5-fluoroorotic acid (FOA), and 2-nitrophenyl-β-D-glucopyranoside (2NPGlc) were obtained from Wako Pure Chemical Industry, Tokyo. Kanamycin sulfate was purchased from Sigma–Aldrich Co., MO, USA.

2.2. *Construction of $hisD_{3110}$, $hisD_{3113}$, and $hisD_{3115}$ mutation allele*

The *hisD* gene encodes the enzyme L-histidinol dehydrogenase. The active site residue His-327 in PEHL motif of *E. coli* HisD protein participates in acid–base catalysis, whereas Glu-326 is responsible for the activation of a water molecule [24]. Since the corresponding Glu-311 in PEHL motif of *T. thermophilus* HisD protein would be expected to be indispensable for catalytic activity, we substituted the amino acid to obtain His auxotroph mutants. About 1800 bp fragment containing *hisD* was amplified by PCR from HB27 DNA and cloned onto pCR4-TOPO. GAG codon for Glu-311 in *hisD* gene was changed to GGG, GCG, or GTG codon for Gly, Ala, and Val, respectively, by site-directed mutagenesis. The HB27 cells were transformed

Table 1 – *Thermus thermophilus* strains used in this study

Strain	Genotype	Source/construction
HB27	wild-type	A. Yamagishi
RT30	$hisD_{3110}$	Mutation at ^{311}Glu (GAG) to Gly (GGG), His$^+$ reversion by G:C to A:T transition
TS7	$hisD_{3110}$, Δ*pyrE*	RT30 × pKN605 (Δ*pyrE*), FOA^r
AYA31	$hisD_{3110}$, *udgA::htk*	RT30 × pHTK366 (*udgA::htk*), Km^r
AYA22	$hisD_{3110}$, *udgB::pyrE*	TS7 × pURA784 (*udgB::pyrE*), Ura$^+$
AYA55	$hisD_{3110}$, *udgA::htk*, *udgB::pyrE*	AYA22 × pHTK366 (*udgA::htk*), Km^r
RT40	$hisD_{3113}$	Mutation at ^{311}Glu (GAG) to Ala (GCG), His$^+$ reversion by C:G to A:T transversion
TS17	$hisD_{3113}$, Δ*pyrE*	RT40 × pKN605 (Δ*pyrE*), FOA^r
TS298	$hisD_{3113}$, *udgB::pyrE*	TS17 × pURA784 (*udgB::pyrE*), Ura$^+$
TS308	$hisD_{3113}$, *udgA::htk*, *udgB::pyrE*	TS298 × pHTK366 (*udgA::htk*), Km^r
RT50	$hisD_{3115}$	Mutation at ^{311}Glu (GAG) to Val (GTG), His$^+$ reversion by T:A to A:T transversion
TS27	$hisD_{3115}$, Δ*pyrE*	RT50 × pKN605 (Δ*pyrE*), FOA^r
TS398	$hisD_{3115}$, *udgB::pyrE*	TS27 × pURA784 (*udgB::pyrE*), Ura$^+$
TS408	$hisD_{3115}$, *udgA::htk*, *udgB::pyrE*	TS398 × pHTK366 (*udgA::htk*), Km^r
WH11	$hisD_{174}$	Mutation at ^{174}Gly (GGG) to Glu (GAG), His$^+$ reversion by A:T to G:C transition [25]
MS8	$hisD_{174}$, Δ*pyrE*	WH11 × pKN605 (Δ*pyrE*), FOA^r
KM709	$hisD_{174}$, *udgB::pyrE*	MS8 × pURA784 (*udgB::pyrE*), Ura$^+$
KM754	$hisD_{174}$, *udgA::htk*, *udgB::pyrE*	KM709 × pHTK366 (*udgA::htk*), Km^r
JOS9	Δ*bgl*	[26]

by homologous recombination with the mutated *hisD* gene fragment on linearized plasmid. His auxotroph mutants were isolated by replica plating method on MSG plates with and without 100 μg/ml His. Introduction of the mutation allele ($hisD_{3110}$ in RT30, $hisD_{3113}$ in RT40, and $hisD_{3115}$ in RT50) in the His auxotroph colonies was confirmed by DNA sequencing. Then 56, 58 and 52 His$^+$ spontaneous revertants were isolated from RT30, RT40, and RT50, respectively, to determine their base-substitutional event. All the His$^+$ revertants restored GAG (Glu) codon from GGG (Glu) in RT30, GCG (Ala) in RT40 or GTG (Val) in RT50. No other base-substitutions such as AGG (Arg), TGG (Trp), CGG (Arg), ACG (Thr), CCG (Pro), and TCG (Ser) were found. Therefore, induction of G:C → A:T, C:G → A:T, and T:A → A:T base-substitutions could be specifically detected in the strain RT30, RT40, and RT50, respectively, by His$^+$ reverse mutations. On the other hand, $hisD_{174}$ allele in WH11 has been identified as a codon change from Gly-174 (GGG) to Glu (GAG) and induction of A:T → G:C transitions could be specifically detected at the target site in our previous study [25].

2.3. *Gene disruption by insertion of htk or pyrE gene cassette*

pKN605 carrying TTC1379-(Δ*pyrE*)-TTC1381 genes and p3TSDN2 carrying the *pyrE* gene cassette (0.6 kbp) were gifts of Dr. M. Tamakoshi (Tokyo University of Pharmacy and Life Science, Japan). An *htk* gene cassette including the promoter region (1.0 kbp) was amplified by PCR from pTAP60 [26] using primers having a *Sac*I site. DNA repair genes (*udgA* and *udgB*) were amplified by PCR from HB27 genomic DNA and subcloned into the plasmid pCR4-TOPO. Then the *Hin*dIII restriction site was incorporated upstream of the *Bam*HI site in the *udgB* gene by PCR for the insertion of the *pyrE* gene fragment. The *htk* gene fragment was inserted into the *Sac*I site in the middle of the *udgA* gene. Transformation of *E. coli* XL1-Blue with the ligated plasmid yielded pHTK366 (*udgA::htk*) and pURA784 (*udgB::pyrE*).

2.4. *Transformation*

Plasmids pHTK366 and pURA784 linearized by *Spe*I or *Nco*I digestion were used for transformation of the *T. thermophilus* strains. A logarithmic growing cell culture (0.5 ml) in PY medium at 70 °C (approx. 1×10^8 cells/ml) was mixed with 25–50 μl of the linearized plasmid DNA solution and cultured for 2 h at 70 °C with gentle shaking to allow homologous recombination. A portion of the culture was spread on PY plates containing 50–100 μg/ml of kanamycin for the selection of transformants containing the *htk* gene. For the selection of *pyrE*$^+$ (Ura$^+$) and Δ*pyrE* (Ura$^-$, FOA^r) transformants, cells were washed with Na–phosphate buffer (10 mM, pH 7.4) by centrifugation and spread on MSG plate supplemented, respectively, with 100 μg/ml His or 100 μg/ml His, 50 μg/ml uracil, and 500 μg/ml FOA. Plates were wrapped in PVC wrapping film and incubated 1–3 days at 70 °C for colony formation. A band of expected size of *udgA::htk* (or *udgB::pyrE*) was amplified by PCR from Km^r (or Ura$^+$) clone, whereas a band of the original size of *udgA* (or *udgB*) was not detected, indicating that the *udgA* (or *udgB*) gene was correctly replaced with *uvrB::htk* (or *udgB::pyrE*) by homologous recombination.

2.5. *Spontaneous His$^+$ reversion frequency*

Independent single colony grown on PY agar plate for 2 days was inoculated into fresh PY medium (OD_{600} = 0.1–0.2) and cultured at 70 °C for additional 4–5 h with shaking (OD_{600} = 0.8–1.6). Cells were washed with Na–phosphate buffer and suspended in buffer at OD_{600} = 1.0. For the measurement of His$^+$ mutants, 0.3 ml was plated onto triplicate MSG plates with 2 ml of top agar. For the determination of viable cells, after 10^{-6} dilution, 0.1-ml was plated onto triplicate PY plates with 2 ml of top agar. Plates were incubated for 2–3 days for MSG plates and 1–2 days for PY plate at 70 °C. Experiments were repeated 3–4 times and total 9 or 13 independent cultures were determined for their mutation frequency.

Mutation rates ($His^+/10^8$/generation) in RT30, AYA31, AYA22, and AYA55 were measured at different growth temperatures, 60, 70, and 78 °C. Bacterial cells grown overnight at 60 °C (OD_{600} = 1.64–2.47) were diluted 1/40-fold with fresh PY medium and cultured at 60, 70, and 78 °C for 8, 6, and 6 h, respectively. The mean number of cell division (n) was calculated from the values of OD_{600}. His^+ mutation frequency ($His^+/10^8$) was measured before and after the cultivation by the method described above using 5 MSG plates for His^+ cells and 5 PY plates for viable cells. All the plates were incubated at 70 °C for colony formation. Mutation rate at 78 °C (MR_{78}) was calculated as $MR_{78} = \{(His^+/10^8$ at 78 °C)—($His^+/10^8$ in preculture at 60 °C)$\}/n$. MR_{70} and MR_{60} were similarly determined. Experiments were conducted twice.

2.6. *Bgl assay*

The plasmid vector pGLS1531 for β-glucosidase (Bgl) reporter assay was described previously [26]. The 5′-upstream region of the *udgA* gene (TTC0366) or the *udgB* gene (TTC0784) was amplified from HB27 chromosomal DNA using PCR primers having 5′-*Aor*13HI and 3′-*Hin*dIII sites. Plasmids pGLS366-1 (*udgA′-bgl*), pGLS366-2 (TTC0367-*udgA′-bgl*), pGLS784-1 (*udgB′-bgl*), and pGLS784-2 (*pccB-udgB′-bgl*) were constructed by replacing the *Aor*13HI-*Hin*dIII region of pGLS1531 with the PCR fragment. Plasmids were introduced into JOS9 (Δ *bgl*) by selection of a Km^r transformant. Bacterial cells were cultured overnight at 70, 74, or 78 °C in PY medium. Bgl activity of toluenized cells was assayed at 80 °C with 2NPGlc as a substrate [26]. Experiments were repeated 3–4 times and mean values were presented in the figures.

3. Results

3.1. *Expression of udgA and udgB genes*

The expression of *udgA* and *udgB* genes was investigated with Bgl reporter assay. It is likely that the *udgA* gene is organized in an operon-like structure with adjacent upstream hypothetical gene TTC0367, because Bgl activity was detected for pGLS366-2 (TTC0367-*udgA′-bgl*) including 5′-upstream region of TTC0367, but not for pGLS366-1 (*udgA′-bgl*) without the region as shown in Fig. 1. Also the *udgB* gene forms an operon-like structure with its upstream gene, *pccB*, because pGLS784-1 (*udgB′-bgl*) lacking 5′-upstream region of *pccB* revealed no Bgl activity (Fig. 1). The pccB gene encodes propionyl-CoA carboxylase beta chain, but the functional correlation with the repair gene *udgB* is not known. Gene expression was almost same level between 70 and 74 °C, but it was decreased at 78 °C, an over-optimal temperature (Fig. 2). The expression levels of *udgA* were about 1.8, 2.4, and 3.4 times that of *udgB* at 70, 74, and 78 °C, respectively. We also investigated the effect of temperature shift-up on the expression of *udgA* and *udgB* genes. An overnight culture at 60 °C was transferred into fresh PY medium and cultured at 70, 74, and 78 °C for 30, 60 and 90 min. Obvious changes in Bgl activity were not observed under the condition, suggesting constitutive gene expression (data not shown).

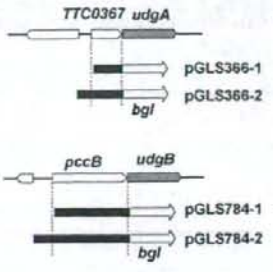

plasmid (JOS9)	Bglactivity (unit/OD600) mean ± SD
–	0.22 ± 0.16
pGLS366-1	0.19 ± 0.04
pGLS366-2	2.34 ± 0.12**
pGLS784-1	0.18 ± 0.06
pGLS784-2	1.47 ± 0.17**

Fig. 1 – Expression of *udgA* and *udgB* gene. Bgl activity was measured for JOS9 (Δ*bgl*) with and without each plasmid. Data are the means of three experiments. The left panel shows a part of *T. thermophilus* genome and the regions of insertion (black bar) into a *bgl* vector. Statistically significant from JOS9 (without plasmid) at $P < 0.01$ (**) by the Dunnett test.

3.2. *Spontaneous hisD reversion frequency*

Two UDG genes, *udgA* and *udgB*, were disrupted by the insertion of *htk* or *pyrE* in 4 different background, $hisD_{174}$, $hisD_{3110}$, $hisD_{3113}$, and $hisD_{3115}$. Deletion of both *udgA* and *udgB* gene was not lethal. Neither obvious growth delay in PY liquid medium nor decrease in colony-forming ability on PY plate of *udgA,B* double mutant was observed at 70 and 74 °C (data not shown). To measure the effect of the *udg* mutation on the frequency of various spontaneous base-substitution mutations, we used the *hisD* reversion system. Spontaneous His^+ mutation frequencies of *udg*-deficient strains were compared with corresponding parent strain WH11, RT30, RT40, or RT50. Concerning the G:C → A:T transitions, the $hisD_{3110}$ reversion frequency of AYA31 (*udgA*) was about 14.7 times that of RT30, while that of AYA22 (*udgB*) was 2.7-fold increase compared with RT30 (Fig. 3). The *udgB* mutant showed weak mutator effect. In contrast to the single *udg* mutant, a pronounced increase in reversion frequency was observed in a double mutant strain AYA55 (*udgA, udgB*). It was about 81.6 times that of RT30. When it was compared between AYA31 (*udgA*)

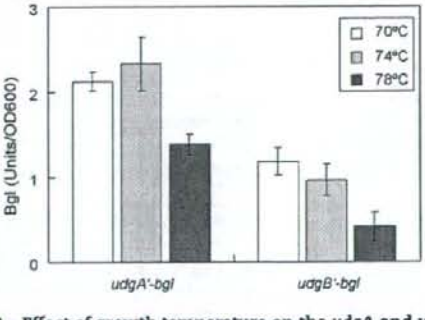

Fig. 2 – Effect of growth temperature on the *udgA* and *udgB* gene expression. JOS9 (Δ*bgl*) cells carrying pGLS366-2 (*udgA′-bgl*) or pGLS784-2 (*udgB′-bgl*) were cultured overnight at 70, 74, or 78 °C. Data are the means of four experiments.

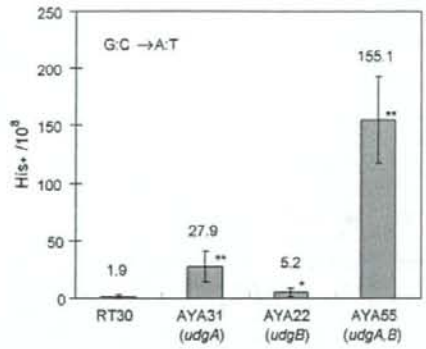

Fig. 3 – Spontaneous mutation frequency of *hisD*$_{3110}$ reversion (G:C → A:T) in *udg* mutants. Values are the mean of 13 independent cultures. Statistically significant from RT30 at $P < 0.05$ (*) or $P < 0.01$ (**) by the Kruskal Wallis test.

and AYA55 (*udgA*, *udgB*), about 5.6-fold increase was observed. The difference would provide the evidence of UdgB activity in a *udgA* background. The results indicated that *udgB* as well as *udgA* gene product played an important role to prevent G:C → A:T transition mutations. Since uracil residues in DNA would not be expected to increase the mutation frequency other than G:C → A:T transitions, we further measured the spontaneous His$^+$ reversion frequencies of *udgA,B* mutants in *hisD*$_{174}$, *hisD*$_{3113}$, or *hisD*$_{3115}$ background. For A:T → G:C transitions, the reversion frequencies of WH11 and KM754 (*udgA,B*) were 0.77 ± 0.59 and $1.22 \pm 0.82 \times 10^{-8}$, respectively (Fig. 4). For C:G → A:T transversions, those of RT40 and TS308 (*udgA,B*) were 3.07 ± 1.22 and $2.24 \pm 2.16 \times 10^{-8}$, respectively. Also those of RT50 and TS408 (*udgA,B*) for T:A → A:T transversions were 1.40 ± 0.63 and $2.02 \pm 1.40 \times 10^{-8}$, respectively. In each comparison, statistical differences were not observed. Thus, deletion of *udgA,B* did not alter the reversion frequencies of the *hisD*$_{174}$, *hisD*$_{3113}$, and *hisD*$_{3115}$ allele as shown in Fig. 4.

As far as investigated, frequency of only G:C → A:T transitions was elevated by the deficiency of *udgA,B* genes. We,

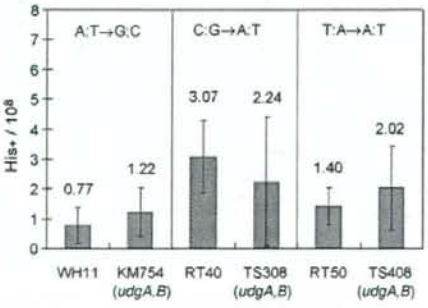

Fig. 4 – Spontaneous mutation frequency of *hisD*$_{174}$ reversion (A:T → G:C), *hisD*$_{3113}$ reversion (C:G → A:T), and *hisD*$_{3115}$ reversion (T:A → A:T) in *udgA,B* mutants and their parent strains. Values are the mean of nine independent cultures.

Table 2 – Mutation rates of G:C to A:T transitions in *udg* mutants cultured at different temperatures

Strain	60 °C culture (start)		Cultured at 60 °C for 8 h				Cultured at 70 °C for 6 h				Cultured at 78 °C for 6 h				
	OD_{600}	His$^+$/10^8	OD_{600}	His$^+$/10^8	n	MR_{60}	Ratio	OD_{600}	His$^+$/10^8	n	MR_{70}	Ratio	OD_{600}	His$^+$/10^8	n	MR_{78}	Ratio
RT30	0.057	0.32	1.12	0.44	4.3	0.028		1.80	1.31	5.0	0.20		1.25	5.05	4.5	1.05	
udg$^+$	0.042	1.28	0.80	1.71	4.3	0.10	1	0.97	2.25	4.5	0.22	1	0.92	28.72	4.5	6.10	1
						(0.064)					(0.21)					(3.58)	
AYA31	0.041	9.90	0.92	11.59	4.5	0.38		1.03	27.44	4.7	3.73		0.70	53.29	4.1	10.58	
udgA	0.040	6.59	0.96	8.61	4.6	0.44	6.4	1.04	13.15	4.7	1.40	12.2	0.92	42.01	4.5	7.87	2.6
						(0.41)					(2.57)					(9.23)	
AYA22	0.052	0.44	1.03	1.09	4.5	0.14		0.89	4.58	4.7	0.88		0.79	18.64	4.1	4.44	
udgB	0.057	2.93	0.99	3.48	4.6	0.12	2.0	1.15	4.39	4.7	0.31	2.9	0.79	20.85	4.5	3.98	1.2
						(0.13)					(0.60)					(4.21)	
AYA55	0.062	83.72	1.05	102.70	4.1	3.17		1.01	154.50	4.1	15.80		0.60	524.20	3.2	135.78	
udgA,B	0.048	43.25	0.86	48.04	4.2	1.14	33.6	1.27	79.26	4.7	7.66	55.9	1.14	495.75	4.6	98.37	32.7
						(2.15)					(11.73)					(117.1)	

Bacterial cultures at 60 °C were diluted 1/40-fold with fresh PY medium and cultured at 60, 70, and 78 °C for 8, 6, and 6 h, respectively. The mean number of cell division (n) was calculated from the values of OD_{600}. MR_{60}, MR_{70}, and MR_{78} represent the mutation rates (His$^+$/10^8/generation) at 60, 70, and 78 °C, respectively. Data of two independent experiments were presented. Values in parentheses were the mean of two experiments.

therefore, further investigated mutation rates in strains RT30, AYA31, AYA22, and AYA55 at different growth temperatures. Cells grown at 60 °C were inoculated into PY medium and cultured at 60, 70, and 78 °C for 6–8 h. The estimated mutation rates of G:C → A:T transitions in *udg*-proficient strain RT30 were 0.064, 0.21, and 3.58 $His^+/10^8$/generation, respectively, at 60, 70, and 78 °C (Table 2). In the absence of *udgA* gene function, they were 0.41, 2.57, and 9.23 $His^+/10^8$/generation at 60, 70, and 78 °C, respectively. Similar temperature-dependent increase in mutation rate was observed in *udgB* strain AYA22. At any temperature the mutation rates were lower than those in *udgA* strain AYA31. Compared with the single mutants, higher mutation rates were observed in AYA55 (*udgA,B*). Their mutation rates at 60, 70, and 78 °C were estimated to be 2.15, 11.73, and 117.1 $His^+/10^8$/generation, respectively. At 70 °C culture, increased ratio of the mutation rate (RT_{70}) compared with the *udg*$^+$ strain was about 12-fold in *udgA*, 3-fold in *udgB*, and 56-fold in *udgA,B* strain. These values were almost same degree as those observed in Fig. 3.

4. Discussion

Deamination of the normal DNA base cytosine to form uracil is one of the major endogenous DNA damages. If the uracil base is not removed before replication, it causes G:C → A:T transition mutations [7]. A mutant of *E. coli* deficient in UDG activity shows an increased rate of spontaneous G:C → A:T mutations [8]. The UDG enzyme system seems to be the universal mechanism for uracil repair, since UDG-homologous genes can be found in a variety of organisms including bacteria, viruses, and eukaryotes. The spontaneous deamination reaction is greatly enhanced at high temperature and, therefore, formation of U:G pre-mutagenic mispair caused by cytosine deamination is particularly profound for extreme thermophiles. Thus, it is plausible that they may have more effective repair systems compared with other mesophiles. *T. thermophilus* has two UDGs, termed UdgA and UdgB. Starkuviene and Fritz [22] reported that UdgA protein belongs to the family of thermostable UDGs and catalyzes the removal of uracil from duplex DNA and single-stranded DNA containing uracil. On the other hand, UdgB, a novel family 5 UDGs, acted on uracil residues in duplex DNA, but not in single-stranded DNA. However, these in vitro assays were performed at 50 °C. It is not known whether these Udg proteins exhibit their enzyme activity at 70 °C or higher. Hoseki et al. [27] have reported crystal structure analysis of UdgA that it removed uracil from DNA in the same manner as did family 1 UDGs. In contrast to the in vitro studies on purified UdgA and UdgB proteins, the role of two enzymes in counteracting the mutagenic threat of cytosine deamination has not been elucidated in vivo at growing temperature.

In the present study, we demonstrated that both the UdgA and UdgB glycosylases prevented mutations caused by cytosine deamination in *T. thermophilus*. MR_{70} of G:C → A:T transitions was stimulated about 56-fold in the *udgA,B* double mutant strain compared with the *udg*$^+$ strain, and about 4.6-fold compared with the *udgA* strain (Table 2). The MR_{70} in *udgB* strain was about 3 times that in the *udg*$^+$ strain. The difference between *udgA* and *udgA,B* strains indicated the function of *udgB* gene in repair of uracil. It is evident that a UdgB glycosylase actually functions in vivo. The temperature-dependent increase in mutation rate in any strain would indicate the enhancement of cytosine deamination at high temperature. Since MR_{78} in the *udg*$^+$ strain was greatly enhanced compared with MR_{70}, repair efficiency of the UdgA and UdgB would be decreased at 78 °C, an over-optimal temperature. It is consistent with the observation that gene expression of *udgA* and *udgB* was also decreased at 78 °C (Fig. 2). Both of the genes seemed to be expressed constitutively. It is unlikely that UdgB acts at higher temperature. On the other hand, other base-substitutions were not affected by the introduction of *udgA,B* mutations. We have not developed other two *hisD* allele for the detection of G:C → C:G and A:T → C:G transversions. However, these types of mutations are known to be comparatively rare event among the base-substitutions found in *E. coli* and *Salmonella typhimurium* [28,29]. Lack of a mismatch repair function (*mutL,H,S*) stimulates G:C → A:T and A:T → G:C transitions, whereas inactivation of repair enzymes for 8-hydroxyguanine (*mutM,Y*) enhances specifically C:G → A:T transversions in *E. coli* [9]. Our *hisD* reversion system developed in the present study would be useful for the investigation of gene functions such as *mutS*, *mutS2*, *mutL*, *mutM*, and *mutY* on mutagenesis in *T. thermophilus*.

Acknowledgments

We thank Drs. Akihiko Yamagishi and Masatada Tamakoshi, Tokyo University of Pharmacy and Life Sciences, for providing bacterial strain HB27 and plasmids. We also thank Rumi Tsunoi for her technical assistance. This work was supported in part by Grants-in Aid for Scientific Research from the Ministry of Education, Science, Sports, and Culture of Japan.

REFERENCES

[1] T. Oshima, K. Imabori, Description of *Thermus thermophilus* (Yoshida and Oshima) comb. nov., a nonsporulating thermophilic bacterium from a Japanese thermal spa, Int. J. Syst. Bacteriol. 24 (1974) 102–112.

[2] S. Yokoyama, Y. Matsuo, H. Hirota, T. Kigawa, M. Shirouzu, Y. Kuroda, H. Kurumizaka, S. Kawaguchi, Y. Ito, T. Shibata, M. Kainosho, Y. Nishimura, Y. Inoue, S. Kuramitsu, Structural genomics projects in Japan, Prog. Biophys. Mol. Biol. 73 (2000) 363–376.

[3] A. Henne, H. Bruggemann, C. Raasch, A. Wiezer, T. Hartsch, H. Liesegang, A. Johann, T. Lienard, O. Gohl, R. Martinez-Arias, C. Jacobi, V. Starkuviene, S. Schlenczeck, S. Dencker, R. Huber, H.P. Klenk, W. Kramer, R. Merkl, G. Gottschalk, H.J. Fritz, The genome sequence of the extreme thermophile *Thermus thermophiles*, Nat. Biotechnol. 22 (2004) 547–553.

[4] Y. Koyama, T. Hoshino, N. Tomizuka, K. Furukawa, Genetic transformation of the extreme thermophilic *Thermus thermophilus* and of other *Thermus* spp., J. Bacteriol. 166 (1986) 338–340.

[5] Y. Koyama, Y. Arikawa, K. Furukawa, A plasmid vector for an extreme thermophile, *Thermus thermophiles*, FEMS Microbiol. Lett. 72 (1990) 97–102.

[6] T. Oshima, M. Baba, Occurrence of *sym*-homospermidine in extremely thermophilic bacteria, Biochem. Biophys. Res. Commun. 103 (1981) 156–160.
[7] B.K. Duncan, J.H. Miller, Mutagenic deamination of cytosine residues in DNA, Nature 287 (1980) 560–561.
[8] B.K. Duncan, B. Weiss, Specific mutator effects of *ung* (uracil-DNA glycosylase) mutations in *Escherichia coli*, J. Bacteriol. 151 (1982) 750–755.
[9] E.C. Friedberg, G.C. Walker, W. Siede, R.D. Wood, R.A. Schultz, T. Ellenberger (Eds.), Base excision repair. In: DNA Repair and Mutagenesis, second ed., ASM Press, Washington, DC, 2006, pp. 169–226.
[10] T. Lindahl, An N-glycosylase from *Escherichia coli* that releases free uracil from DNA containing deaminated cytosine residues, Proc. Natl. Acad. Sci. U.S.A. 71 (1974) 3649–3653.
[11] L.H. Pearl, Structure and function in the uracil-DNA glycosylase superfamily, Mutat. Res. 460 (2000) 165–181.
[12] P. Gallinari, J. Jiricny, A new class of uracil-DNA glycosylases related to human thymine-DNA glycosylase from HeLa cells, Nature 383 (1996) 735–738.
[13] P. Neddermann, J. Jiricny, Efficient removal of uracil from G:U mispairs by the mismatch-specific thymine DNA glycosylase from HeLa cells, Proc. Natl. Acad. Sci. U.S.A. 91 (1994) 1642–1646.
[14] M. Saparbaev, J. Laval, 3,N^4-ethenocytosine, a highly mutagenic adduct, is a primary substrate for *Escherichia coli* double-stranded uracil-DNA glycosylase and human mismatch-specific thymine DNA glycosylase, Proc. Natl. Acad. Sci. U.S.A. 95 (1998) 8508–8513.
[15] E. Lutsenko, A.S. Bhagwat, The role of the *Escherichia coli* Mug protein in the removal of uracil and 3, N^4-ethenocytosine from DNA, J. Biol. Chem. 274 (1999) 31034–31038.
[16] R.J. Boorstein, A. Cummings Jr., D.R. Marenstein, M.K. Chan, Y. Ma, T.A. Neubert, S.M. Brown, G.W. Teebor, Definitive identification of mammalian 5-hydroxymethyluracil DNA *N*-glycosylase activity as SMUG1, J. Biol. Chem. 276 (2001) 41991–41997.
[17] H.S. Pettersen, O. Sundheim, K.M. Gilljam, G. Slupphaug, H.E. Krokan, B. Kavli, Uracil-DNA glycosylases SMUG1 and UNG2 coordinate the initial steps of base excision repair by distinct mechanisms, Nucleic Acids Res. 35 (2007) 3879–3892.
[18] M. Sandigursky, A. Faje, W.A. Franklin, Characterization of the full length uracil-DNA glycosylase in the extreme thermophile *Thermotoga maritima*, Mutat. Res. 485 (2001) 187–195.
[19] M. Sandigursky, W.A. Franklin, Uracil-DNA glycosylase in the extreme thermophile *Archaeoglobus fulgidus*, J. Biol. Chem. 275 (2000) 19146–19149.
[20] A.A. Sartori, P. Schar, S. Fitz-Gibbon, J.H. Miller, J. Jiricny, Biochemical characterization of uracil processing activities in the hyperthermophilic archaeon *Pyrobaculum aerophilum*, J. Biol. Chem. 276 (2001) 29979–29986.
[21] A.A. Sartori, S. Fitz-Gibbon, H. Yang, J.H. Miller, J. Jiricny, A novel uracil-DNA glycosylase with broad substrate specificity and an unusual active site, EMBO J. 21 (2002) 3182–3191.
[22] V. Starkuviene, H.J. Fritz, A novel type of uracil-DNA glycosylase mediating repair of hydrolytic DNA damage in the extremely thermophilic eubacterium *Thermus thermophiles*, Nucleic Acids Res. 30 (2002) 2097–2102.
[23] J.H. Chung, E.K. Im, H.Y. Park, J.H. Kwon, S. Lee, J. Oh, K.C. Hwang, J.H. Lee, Y. Jang, A novel uracil-DNA glycosylase family related to the helix-hairpin-helix DNA glycosylase superfamily, Nucleic Acids Res. 31 (2003) 2045–2055.
[24] J.A.R.G. Barbosa, J. Sivaraman, Y. Li, R. Larocque, A. Matte, J.D. Schrag, M. Cygler, Mechanism of action and NAD^+-binding mode revealed by the crystal structure of L-histidinol dehydrogenase, Proc. Natl. Acad. Sci. U.S.A. 99 (2002) 1859–1864.
[25] T. Ohta, S. Tokishita, K. Mochizuki, J. Kawase, M. Sakahira, H. Yamagata, UV sensitivity and mutagenesis of the extremely thermophilic eubacterium *Thermus thermophilus* HB27, Genes Environ. 28 (2006) 56–61.
[26] T. Ohta, S. Tokishita, R. Imazuka, I. Mori, J. Okamura, H. Yamagata, β-Glucosidase as a reporter for the gene expression studies in *Thermus thermophilus* and constitutive expression of DNA repair genes, Mutagenesis 21 (2006) 255–260.
[27] J. Hoseki, A. Okamoto, R. Masui, T. Shibata, Y. Inoue, S. Yokoyama, S. Kuramitsu, Crystal structure of a family 4 uracil-DNA glycosylase from *Thermus thermophilus* HB8, J. Mol. Biol. 333 (2003) 515–526.
[28] M. Watanabe-Akanuma, R. Woodgate, T. Ohta, Enhanced generation of A:T → T:A transversions in a *recA730 lexA*(Def) mutant of *Escherichia coli*, Mutation Res. 373 (1997) 61–66.
[29] T. Ohta, M. Watanabe-Akanuma, H. Yamagata, A comparison of mutation spectra detected by the *Escherichia coli* Lac^+ reversion assay and the *Salmonella typhimurium* His^+ reversion assay, Mutagenesis 15 (2000) 317–323.

Oxidative DNA Damage in *XPC*-Knockout and Its Wild Mice Treated with Equine Estrogen

Yoshinori Okamoto,[†] Pei-Hsin Chou,[‡] Sung Yeon Kim,[†,§] Naomi Suzuki,[†] Y. R. Santosh Laxmi,[†] Kanako Okamoto,[†] Xiaoping Liu,[†] Tomonari Matsuda,[‡] and Shinya Shibutani*[,†]

Laboratory of Chemical Biology, Department of Pharmacological Sciences, State University of New York at Stony Brook, Stony Brook, New York 11794-8651, and Research Center for Environmental Quality Management, Kyoto University, Otsu, Shiga, 520-0811, Japan

Received December 6, 2007

Long-term hormone replacement therapy with equine estrogens is associated with a higher risk of breast, ovarian, and endometrial cancers. Reactive oxygen species generated through redox cycling of equine estrogen metabolites may damage cellular DNA. Such oxidative stress may be linked to the development of cancers in reproductive organs. Xeroderma pigmentosa complementation group C-knockout (*Xpc*-KO) and wild-type mice were treated with equilenin (EN), and the formation of 7,8-dihydro-8-oxodeoxyguanosine (8-oxodG) was determined as a marker of typical oxidative DNA damage, using liquid chromatography electrospray tandem mass spectrometry. The level of hepatic 8-oxodG in wild-type mice treated with EN (5 or 50 mg/kg/day) was significantly increased by approximately 220% after 1 week, as compared with mice treated with vehicle. In the uterus also, the level of 8-oxodG was significantly increased by more than 150% after 2 weeks. Similar results were observed with *Xpc*-KO mice, indicating that *Xpc* does not significantly contribute to the repair of oxidative damage. Oxidative DNA damage generated by equine estrogens may be involved in equine estrogen carcinogenesis.

Introduction

Hormone replacement therapy (HRT)[1] is widely used by postmenopausal women to alleviate menopausal symptoms and to protect against osteoporosis. In the United States, more than 40% of women in this demographic currently receive HRT, with Premarin (Wyeth-Ayerst) being one of the most commonly used products (*1*). However, HRT is associated with a significantly increased risk of breast, ovarian, and endometrial cancers (*2–4*). Premarin, composed of approximately 30% equilin (EQ), 10% equilenin (EN), and other estrogens, is frequently used for this purpose (*1*). Like human estrogens, EN and EQ are hydroxylated to 4-hydroxyequilenin (4-OHEN) and 4-hydroxyequilin (4-OHEQ), respectively (*1*) (Figure 1). 4-OHEN is rapidly autoxidized to an *o*-quinone, which reacts readily with DNA in vitro, resulting in the formation of bulky DNA adducts (*1, 5, 6*). 4-OHEQ is also autoxidized to an *o*-quinone that isomerizes to 4-OHEN-*o*-quinone; therefore, 4-OHEQ produces DNA adducts identical to those generated by 4-OHEN (*7*). Mutagenic events induced by 4-OHEQ were observed in a *supF* shuttle vector plasmid propagated in human cells (*8*). 4-OHEN-induced DNA adducts were highly miscoded during translesion synthesis catalyzed by human DNA polymerases (*9–11*). Equine estrogen-derived DNA adducts have been detected in the mammary fat pads of rats treated with 4-OHEN (*12*), in breast tumor and adjacent normal tissues of several patients receiving HRT, and in paraffin-embedded breast tumor tissues (*13*).

Redox cycling between the *o*-quinone of 4-OHEN and its semiquinone radical generates reactive oxygen species (ROS) such as superoxide, hydrogen peroxide, and ultimately reactive hydroxyl radicals (*14*) (Figure 1). When 4-OHEN was incubated with DNA or exposed to breast cancer cells in culture, increased formation of 7,8-dihydro-8-oxodeoxyguanosine (8-oxodG) lesions, a typical marker of oxidative DNA damage, was detected (*14–18*). Similar phenomena were observed when 4-OHEN was injected directly into the mammary fat pads of rats (*12*). 8-OxodG is a miscoding and mutagenic lesion (*19–21*). Therefore, oxidative DNA damage induced by equine estrogens may also be involved in carcinogenesis. If equine estrogens produce mutagenic DNA lesions in breast, ovarian, and endometrial tissues of women receiving HRT, such mutagenic DNA adducts may contribute to the initiation of these cancers. The equine estrogen-derived DNA adducts therefore provide biomarkers useful in evaluating the risk of HRT on an individual basis.

Xpc-knockout (*Xpc*-KO) mice are deficient in both alleles of mouse xeroderma pigmentosum complementation group C, one of several factors involved in the recognition of a variety of bulky DNA-distorting lesions in nucleotide excision repair (*22*). Recently, a reduction in the rate of repair of 8-oxodG was observed in human keratinocytes and fibroblasts lacking *Xpc*, indicating that *Xpc* plays an unexpected and multifaceted role in cell protection from oxidative DNA damage (*23*).

To explore the oxidative DNA damage induced by equine estrogens in animals, female mice were treated orally with EN. The levels of 8-oxodG in the liver and uterus were determined

* To whom correspondence should be addressed. Tel: 631-444-7849. Fax: 631-444-3218. E-mail: shinya@pharm.stonybrook.edu.
[†] SUNY at Stony Brook.
[‡] Kyoto University.
[§] Present address: Department of Pharmacy, Wonkwang University, Iksan Chonbuk 570-709, South Korea.

[1] Abbreviations: HRT, hormone replacement therapy; EQ, equilin; EN, equilenin; 4-OHEQ, 4-hydroxyequilin; 4-OHEN, 4-hydroxyequilenin; 8-oxodG, 8-oxo-7,8-dihydro-2′-deoxyguanosine; dNTP, 2′-deoxynucleoside triphosphate; ROS, reactive oxygen species; *Xpc*, xeroderma pigmentosa complementation group C; PAGE, polyacrylamide gel electrophoresis; HPLC, high-performance liquid chromatography; LC/MS/MS, liquid chromatography electrospray tandem mass spectrometry.

10.1021/tx700428m CCC: $40.75
Published on Web 05/01/2008

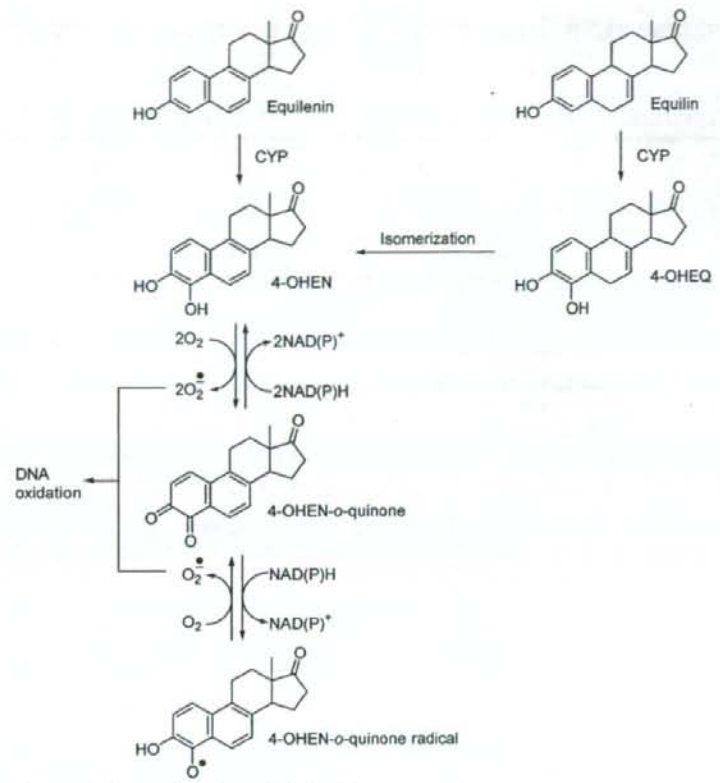

Figure 1. DNA damage and redox cycling mediated through 4-OHEN.

using liquid chromatography electrospray tandem mass spectrometry (LC/MS/MS). Liver was chosen as a major organ metabolizing EN, and uterus was chosen as one of target reproductive organs developing cancer. To evaluate the contribution of *Xpc* in the removal of oxidative DNA damage, EN was also administered to *Xpc*-KO mice. The level of 8-oxodG observed in *Xpc*-KO mice was compared with that observed in wild-type B6129F1 mice.

Materials and Methods

Materials. EN was purchased from Steraloids Inc. (Wilton, NH). 4-OHEN was prepared as described previously (*10*). Desferrioxamine and alkaline phosphatase were obtained from Sigma-Aldrich (St. Louis, MO). $^{15}N_5$-dG was purchased from Cambridge Isotope Laboratory (Andover, MA). Nuclease P1 was obtained from Roche Applied Science (Indianapolis, IN).

Animal Studies. The use of animals was in compliance with the guidelines established by the NIH Office of Laboratory Animal Welfare. *Xpc*-KO mice and mice of the wild-type progenitor strain, B6129F1 (female, 6 weeks old), were purchased from Taconic (Germantown, NY). Animals were acclimated in temperature (22 ± 2 °C) and humidity (55 ± 5%) controlled rooms with a 12 h light−dark cycle for at least 1 week prior to use. Regular laboratory chow and tap water were allowed ad lib. Mice were treated orally (p.o.) with EN (5 or 50 mg/kg/day) for 1 or 2 weeks. Control mice were treated with an identical volume of corn oil. Mice were euthanized by CO_2 asphyxiation at 24 h after the final treatment and then subjected to open thoracotomy. The liver and uterus were removed quickly, frozen, and stored at −80 °C until DNA extraction.

Preparation of DNA Samples. DNA was extracted from the tissue by a modified method of Wang et al. (*24*). To prevent artifactual 8-oxodG formation during DNA extraction, desferrioxamine was used as an antioxidant, as demonstrated in interlaboratory validation study organized by the European Standards Committee on Oxidative DNA Damage (*25*). The tissue (100 mg) was homogenized at 4 °C in 0.2 mL of lysis solution A (320 mM sucrose, 5 mM $MgCl_2$, 10 mM Tris-HCl, 0.1 mM desferrioxamine, pH 7.5, and 1% Triton X-100) using a disposable pellet pestle (Kimble/Kontes, Vineland, NJ). After the tissue was ground, the homogenate was subjected to centrifugation at 10000*g* for 20 s at 4 °C. One milliliter of lysis solution A was added to the pellet and agitated by vortexing. These steps were repeated twice. After centrifugation, 200 μL of solution B (10 mM Tris-HCl, 5 mM EDTA-Na_2, and 0.15 mM desferrioxamine, pH 8.0) and 20 μL of 10% SDS were added to the pellet. The mixture was vortexed for 10 s and incubated at 37 °C for 10 min for suspension of the pellet and to allow for complete lysis of the nuclear membrane. After the addition of 2.7 μg of RNase T_1 and 10 μg of RNase A in a buffer (10 mM Tris-HCl, 1 mM EDTA, and 2.5 mM desferrioxamine, pH 7.4), the samples were incubated at 50 °C for 15 min. Following incubation, 10 μL of Qiagen proteinase K solvent was added, and the samples were incubated for 1 h at 37 °C. After the addition of 0.3 mL of NaI solution (7.6 M NaI, 40 mM Tris-HCl, 20 mM EDTA-Na_2, and 0.3 mM desferrioxamine, pH 8.0), DNA was precipitated by the addition of 500 μL of 2-propanol. The DNA lump was fished out and washed twice with 40% 2-propanol. Finally, the recovered DNA was dried and dissolved in 500 μL of distilled water. The concentration of DNA was determined by UV spectroscopy as 50 μg/mL = $O.D._{260nm}$ 1.0.

Determination of 8-OxodG by LC/MS/MS Analysis. The level of 8-oxodG was determined using LC/MS/MS [high-performance liquid chromatography (HPLC), a Shimadzu LC-10ADvp pump and SIL-10AD autoinjector; MS/MS, Waters-Micromass Quattro Ultima Pt Triple Quadrupole mass spectrometer]. To quantify

8-oxodG accurately, $^{15}N_5$-8-oxodG was prepared from $^{15}N_5$-dG, whose all five Ns in the guanine base were replaced by ^{15}N (Cambridge Isotope Laboratory), following a method developed previously (*26*), and used as an internal standard. The DNA (25 μg) was mixed with $^{15}N_5$-8-oxodG (500 pg) and digested at 37 °C for 3 h with nuclease P1 (4 unit) in 114 μL of buffer mixture [100 μL of 30 mM sodium acetate buffer containing 10 mM 2-mercaptoethanol, pH 5.3; 5 μL of 20 mM $ZnSO_4$; 5 μL of $^{15}N_5$-8-oxodG solution (5 ng/mL); 4 μL of nuclease P1 solution (1 unit/μL); and 3 units of alkaline phosphatase]. After incubation, 20 μL of 0.5 M Tris-HCl, pH 8.5, was added and incubated for 3 h. The enzymes were methanol-precipitated, and the supernatant containing the nucleoside was evaporated and reconstituted with 100 μL of water.

The LC column was eluted over a gradient that began at a ratio of 2% methanol to 98% water and was changed to 40% methanol over a period of 40 min, changed to 80% methanol from 40 to 45 min, and finally returned to the original starting conditions, 2:98, for the remaining 15 min. The total run time was 60 min. Sample injection volumes of 50 μL each were separated on a Shim-pack FC-ODS column (150 mm × 4.6 mm) and eluted at a flow rate of 0.4 mL/min. Mass spectral analyses were carried out in positive ion mode with nitrogen as the nebulizing gas. The ion source temperature was 130 °C, the desolvation gas temperature was 380 °C, and the cone voltage was operated at a constant 40 V. Nitrogen gas was also used as the desolvation gas (700 L/h) and cone gas (35 L/h), and argon was used as the collision gas at a collision cell pressure of 1.5×10^{-3} mBar. Positive ions were acquired in MRM mode. The MRM transitions were monitored as follows: $^{15}N_5$-8-oxodG (*m/z* 288.8 → 172.8) and 8-oxodG (*m/z* 283.8 → 167.8), respectively. The level of 8-oxodG in the DNA samples was determined by comparing with $^{15}N_5$-8-oxodG. The detection limit was approximately 0.1 adducts in 10^6 bases using 25 μg of DNA. The amount of dG in the DNA digest was monitored by a Simadzu SPD-10A UV−visible detector prior to MS/MS analysis. The level of 8-oxodG lesions was estimated by the following equation: the level of 8-oxodG lesion = (amount of 8-oxodG)/[(amount of dG) × 4].

Statistical Analysis. Results were expressed as means ± standard deviations (SDs). A two-sided student's *t* test was used to evaluate the difference. Values of $p \leq 0.05$ were considered statistically significant from the control group.

Results

The level of 8-oxodG lesions in B6129F1 mice treated p.o. with EN was determined using LC/MS/MS analysis and an internal standard, $^{15}N_5$-8-oxodG (Figure 2). The detection limit for 25 μg of DNA sample was approximately 0.1 adduct/10^6 nucleotides. The level of 8-oxodG in the livers of mice treated with 5 mg/kg EN was significantly increased, 220% after 1 week (6.3 adducts/10^6 nucleotides) and 170% after 2 weeks (4.9 adducts/10^6 nucleotides), as compared with that of mice treated with vehicle (2.9 adducts/10^6 nucleotides) (Table 1). With 50 mg/kg EN treatment, a high level of hepatic 8-oxodG (222%) ($p < 0.01$) was also observed after 1 week; however, no significant increase was detected after 2 weeks.

In the uterus, the background level of 8-oxodG was 3.9 times higher than that observed in the liver (Table 1). Although no significant difference was observed after 1 week of treatment with 5 and 50 mg/kg EN, the levels of uterine 8-oxodG were significantly increased after 2 weeks of treatment, to 150 and 162%, respectively, of the background level.

When *Xpc*-KO mice were treated for 1 week with 5 and 50 mg/kg EN, the hepatic 8-oxodG levels increased 155 and 283%, respectively (Table 1); however, no significant increase of 8-oxodG was detected after 2 weeks, as observed with the wild-type mice. The increases of 8-oxodG level in the wild-type and *Xpc*-KO mice treated for 1 week with 50 mg/kg EN were 3.5 ± 1.0 and 8.8 ± 0.4 adducts/10^6 nucleotides, respectively, when their control levels were subtracted. The 8-oxodG increase in *Xpc*-KO mice was 2.5 times higher than that observed in the wild-type mice ($p < 0.01$). The levels of uterine 8-oxodG were significantly increased to 159 (15.7 adducts/10^6 nucleotides) and 193% (19.1 adducts/10^6 nucleotides) after 2 weeks of treatment with 5 and 50 mg/kg EN, as observed with the wild-type mice.

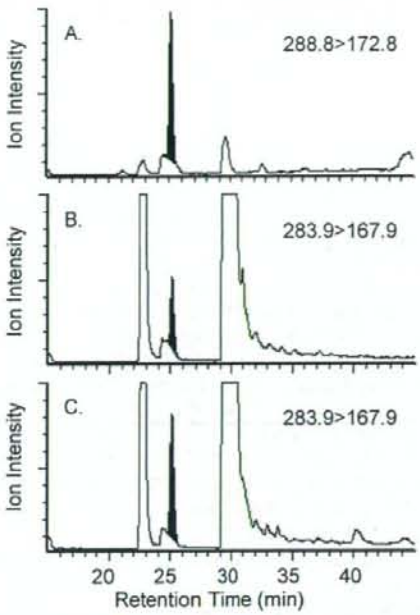

Figure 2. LC/MS/MS analysis of 8-oxodG. The DNA (25 μg) was mixed with $^{15}N_5$-8-oxodG (500 pg) and digested with nuclease P1 and alkaline phosphatase in a buffer. The resulting nucleosides were analyzed using LC/MS/MS, as described in the Materials and Methods. Quantitative analysis of $^{15}N_5$-8-oxodG and 8-oxodG was achieved by monitoring the MS/MS transitions corresponding to the loss of deoxyribose from $^{15}N_5$-8-oxodG (*m/z* 288.8 → 172.8) and 8-oxodG (*m/z* 283.8 → 167.8), respectively. By comparing with internal standard $^{15}N_5$-8-oxodG (A), the level of 8-oxodG in hepatic DNA samples from *Xpc*-KO mouse treated with a vehicle (B) or EN (5 mg/kg/day, p.o. for 2 weeks) (C) was determined.

Table 1. Levels of Hepatic and Uterine 8-OxodG in *Xpc*-KO and Wild-Type Mice Treated Orally with EN

	dose (mg/kg)	duration (weeks)	8-oxodG (adducts/10^6 dNs) wild type	8-oxodG (adducts/10^6 dNs) *Xpc*-KO
			liver	
control			2.9 ± 0.5[a] (100)[b]	4.8 ± 2.4[a] (100)[b]
EN	5.0	1	6.3 ± 1.6* (220)	7.4 ± 3.7 (155)
		2	4.9 ± 2.0* (170)	5.3 ± 0.9 (110)
	50	1	6.4 ± 1.4** (222)	13.6 ± 0.4** (283)
		2	3.4 ± 1.4 (117)	7.7 ± 3.9 (160)
			uterine	
control			11.2 ± 2.2[a] (100)[b]	9.9 ± 4.1[a] (100)[b]
EN	5.0	1	12.9 ± 1.3 (115)	12.1 ± 1.3 (122)
		2	16.8 ± 3.9** (150)	15.7 ± 0.7* (159)
	50	1	11.8 ± 1.1 (105)	10.9 ± 1.6 (110)
		2	18.1 ± 5.4* (162)	19.1 ± 6.4* (193)

[a] Data are expressed as mean values ± SD from three mice in the EN-treated groups and six mice in the control groups. *t* test: *$p < 0.05$ and **$p < 0.01$. [b] The numbers in brackets are % values relative to the control level.

Discussion

Many chemicals, including polycyclic aromatic hydrocarbons and estrogens, are metabolically activated to form quinones. ROS such as superoxide, hydrogen peroxide, and, ultimately, reactive hydroxyl radicals are generated through redox cycling between the *o*-quinone and its semiquinone radical and attack cellular macromolecules, including DNA, to generate oxidative DNA damage such as 8-oxodG (*27*). Similarly, 4-OHEN, a major metabolite of EN, autoxidizes to the *o*-quinone without enzymatic or metal ion catalysis (*7*). ROS generated during redox cycling between 4-OHEN-*o*-quinones and their semiquinones cause oxidative DNA damage; indeed, increased formation of 8-oxodG was observed when calf thymus DNA was reacted directly with 4-OHEN (*14*). In mice treated orally with EN, significant increases of 8-oxodG were observed in the liver and uterus using LC/MS/MS (Table 1). A similar result was observed when 4-OHEN was injected directly into the mammary fat pads of rats (*12*). These results indicated that oxidative DNA damage occurs in reproductive organs. ROS generated by equine estrogen and its metabolite may contribute to the process of equine estrogen carcinogenesis.

Women receiving HRT take Premarin at a dose 0.625 (~0.01 mg/kg/day) or 1.25 mg/day (~0.021 mg/kg/day). Because equine estrogens present in Premarin are approximately 40%, women get equine estrogens 0.004 or 0.0084 mg/kg/day. Although the doses (5.0 and 50 mg/kg/day) used in this animal experiment were in excess than the daily dose for women, women receive HRT over 5 years. Therefore, to determine the capability of forming EN-induced oxidative DNA damage in a short period (1 or 2 weeks), high doses were used in this experiment, as reported that other research groups treated a high dose of 4-OHEN (3.1 mg/kg) to rats (*12*). Although the increases of hepatic and uterine 8-oxodG level were observed with both the wild-type and the *Xpc*-KO mice, the 8-oxodG level for 50 mg/kg EN treatment was similar or slightly higher than that observed with 5 mg/kg EN treatment. Such excessive EN doses may give overcapacity for the metabolizing enzymes to produce 4-OHEN, a precursor of forming ROS. The high level of hepatic 8-oxodG observed after 1 week of treatment (5.0 or 50 mg/kg) was subsequently decreased at 2 week. The decrease of hepatic 8-oxodG over time may occur by repair enzymes induced after EN treatment. Our results encourage treating animals for longer periods with low EN doses for predicting the capability of forming oxidative damage in women.

Xpc is a factor involved in the recognition of a variety of bulky DNA-distorting lesions in nucleotide excision repair (*22*) and may also be associated with repair of 8-oxodG (*23*). If *Xpc* is involved in the repair of 8-oxodG, then the lesions should remain in the tissues of *Xpc*-KO mice for considerably longer than in the tissues of wild-type mice. When EN was administered to both *Xpc*-KO and wild-type mice, a significantly higher formation of 8-oxodG was detected only in liver of *Xpc*-KO mice treated with 50 mg/kg; no significant difference in 8-oxodG levels was observed between them with other doses and/or tissues (Table 1). Our results indicate that *Xpc* may not have a primary role in the repair of 8-oxodG.

In *Xpc*-KO and wild-type mice treated only with the vehicle, the levels of 8-oxodG in the uterus were 3.9 and 2.1 times, respectively, higher than that observed in the liver. The uterus is a principal producer of steroid hormones, including estrogen. Estrogen metabolites are known to produce free radicals during redox cycling, generating oxidative DNA damage, including 8-oxodG (*28*). ROS generated by steroid metabolites may be the cause of the increased background level of 8-oxodG in the uterus.

In conclusion, our results indicate that oxidative DNA damage induced by equine estrogen in reproductive organs may contribute to the process of equine estrogen carcinogenesis and increase the risk of developing reproductive cancer in women receiving HRT.

Acknowledgment. This study was supported by Grant ES012408 from the National Institute of Environmental Health Sciences, Grants-in-Aid for scientific research 18101003 from the Ministry of Education, Culture, Sports, Science and Technology of Japan, and Grants-in-Aid for scientific research from the Ministry of Health, Labor and Welfare of Japan.

References

(1) Bolton, J. L., Pisha, E., Zhang, F., and Qiu, S. (1998) Role of quinoids in estrogen carcinogenesis. *Chem. Res. Toxicol. 11*, 1113–1127.
(2) Colditz, G. A., Hankinson, S. E., Hunter, D. J., Willett, W. C., Manson, J. E., Stampfer, M. J., Hennekens, C. H., Rosner, B., and Speizer, F. E. (1995) The use of estrogens and progestins and the risk of breast cancer in postmenopausal women. *N. Engl. J. Med. 332*, 1589–1593.
(3) Grodstein, F., Stampfer, M. J., Colditz, G. A., Willett, W. C., Manson, J. E., Joffe, M., Rosner, B., Fuchs, C., Hankinson, S. E., Hunter, D. J., Hennekens, C. H., and Speizer, F. E. (1997) Postmenopausal hormone therapy and mortality. *N. Engl. J. Med. 336*, 1769–1775.
(4) Lacey, J. V., Jr., Mink, P. J., Lubin, J. H., Sherman, M. E., Troisi, R., Hartge, P., Schatzkin, A., and Schairer, C. (2002) Menopausal hormone replacement therapy and risk of ovarian cancer. *J. Am. Med. Assoc. 288*, 334–341.
(5) Shen, L., Qiu, S., Chen, Y., Zhang, F., van Breemen, R. B., Nikolic, D., and Bolton, J. L. (1998) Alkylation of 2′-deoxynucleosides and DNA by the Premarin metabolite 4-hydroxyequilenin semiquinone radical. *Chem. Res. Toxicol. 11*, 94–101.
(6) Ding, S., Shapiro, R., Geacintov, N. E., and Broyde, S. (2003) Conformations of stereoisomeric base adducts to 4-hydroxyequilenin. *Chem. Res. Toxicol. 16*, 695–707.
(7) Zhang, F., Chen, Y., Pisha, E., Shen, L., Xiong, Y., van Breemen, R. B., and Bolton, J. L. (1999) The major metabolite of equilin, 4-hydroxyequilin, autoxidizes to an *o*-quinone which isomerizes to the potent cytotoxin 4-hydroxyequilenin-*o*-quinone. *Chem. Res. Toxicol. 12*, 204–213.
(8) Yasui, M., Matsui, S., Laxmi, Y. R. S., Suzuki, N., Kim, S. Y., Shibutani, S., and Matsuda, T. (2003) Mutagenic events induced by 4-hydroxyequilin in *supF* shuttle vector plasmid propagated in human cells. *Carcinogenesis 24*, 911–917.
(9) Suzuki, N., Yasui, M., Laxmi, Y. R. S., Ohmori, H., Hanaoka, F., and Shibutani, S. (2004) Translesion synthesis past equine estrogen-derived 2′-deoxycytidine DNA adducts by human DNA polymerases η and κ. *Biochemistry 43*, 11312–11320.
(10) Yasui, M., Laxmi, Y. R. S., Ananthoju, S. R., Suzuki, N., Kim, S. Y., and Shibutani, S. (2006) Translesion synthesis past equine estrogen-derived 2′-deoxyadenosine DNA adducts by human DNA polymerases η and κ. *Biochemistry 45*, 6187–6194.
(11) Yasui, M., Suzuki, N., Liu, X., Okamoto, Y., Kim, S. Y., Laxmi, Y. R. S., and Shibutani, S. (2007) Mechanism of translesion synthesis past an equine estrogen-DNA adduct by Y-family DNA polymerases. *J. Mol. Biol. 371*, 1151–1162.
(12) Zhang, F., Swanson, S. M., van Breemen, R. B., Liu, X., Yang, Y., Gu, C., and Bolton, J. L. (2001) Equine estrogen metabolite 4-hydroxyequilenin induces DNA damage in the rat mammary tissues: Formation of single-strand breaks, apurinic sites, stable adducts, and oxidized bases. *Chem. Res. Toxicol. 14*, 1654–1659.
(13) Embrechts, J., Lemiere, F., Van Dongen, W., Esmans, E. L., Buytaert, P., Van Marck, E., Kockx, M., and Makar, A. (2003) Detection of estrogen DNA-adducts in human breast tumor tissue and healthy tissue by combined nano LC-nano ES tandem mass spectrometry. *J. Am. Soc. Mass Spectrom. 14*, 482–491.
(14) Chen, Y., Shen, L., Zhang, F., Lau, S. S., van Breemen, R. B., Nikolic, D., and Bolton, J. L. (1998) The equine estrogen metabolite 4-hydroxyequilenin causes DNA single-strand breaks and oxidation of DNA bases in vitro. *Chem. Res. Toxicol. 11*, 1105–1111.
(15) Han, X., and Liehr, J. G. (1995) Microsome-mediated 8-hydroxylation of guanine bases of DNA by steroid estrogens: Correlation of DNA damage by free radicals with metabolic activation to quinones. *Carcinogenesis 16*, 2571–2574.

(16) Chen, Y., Liu, X., Pisha, E., Constantinou, A. I., Hua, Y., Shen, L., van Breemen, R. B., Elguindi, E. C., Blond, S. Y., Zhang, F., and Bolton, J. L. (2000) A metabolite of equine estrogens, 4-hydroxyequilenin, induces DNA damage and apoptosis in breast cancer cell lines. *Chem. Res. Toxicol. 13*, 342–350.

(17) Zhang, F., Yao, D., Hua, Y., van Breemen, R. B., and Bolton, J. L. (2001) Synthesis and reactivity of the catechol metabolites from the equine estrogen, 8,9-dehydroestrone. *Chem. Res. Toxicol. 14*, 754–763.

(18) Liu, X., Yao, J., Pisha, E., Yang, Y., Hua, Y., van Breemen, R. B., and Bolton, J. L. (2002) Oxidative DNA damage induced by equine estrogen metabolites: Role of estrogen receptor α. *Chem. Res. Toxicol. 15*, 512–519.

(19) Shibutani, S., Takeshita, M., and Grollman, A. P. (1991) Insertion of specific bases during DNA synthesis past the oxidation-damaged base 8-oxodG. *Nature 349*, 431–434.

(20) Moriya, M. (1993) Single strand shuttle phagemid for mutagenesis studies in mammalian cells: 8-oxoguanine in DNA induces targeted G:C → T:A transversion in simian kidney cells. *Proc. Natl. Acad. Sci. U.S.A. 90*, 1122–1126.

(21) Tan, X., Grollman, A. P., and Shibutani, S. (1999) Comparison of the mutagenic properties of 8-oxo-7,8-dihydro-2′-deoxyadenosine and 8-oxo-7,8-dihydro-2′-deoxyguanosine DNA lesions in mammalian cells. *Carcinogenesis 20*, 2287–2292.

(22) Sands, A. T., Abuin, A., Sanchez, A., Conti, C. J., and Bradley, A. (1995) High susceptibility to ultraviolet-induced carcinogenesis in mice lacking XPC. *Nature 14*, 162–165.

(23) D'Errico, M., Parlanti, E., Teson, M., Bernardes de Jesus, B. M., Degan, P., Calcagnile, A., Jaruga, P., Bjørås, M., Crescenzi, M., Pedrini, A. M., Egly, J., Zambruno, G., Stefanini, M., Dizdaroglu, M., and Dogliotti, E. (2006) New functions of XPC in the protection of human skin cells from oxidative damage. *EMBO J. 25*, 4305–4315.

(24) Wang, L., Hirayasu, K., Ishizawa, M., and Kobayashi, Y. (1994) Purification of genomic DNA from human whole blood by isopropanol-fractionation with concentrated NaI and SDS. *Nucleic Acids Res. 22*, 1774–1775.

(25) Collins, A., and Gedik, C. M. (2005) Establishing the background level of base oxidation in human lymphocyte DNA: results of an interlaboratory validation study ESCODD (European Standards Committee on Oxidative DNA Damage). *FASEB J. 19*, 82–84.

(26) Schuler, D., Otteneder, M., Sagelsdorff, P., Eder, E., Gupta, R. C., and Lutz, W. K. (1997) Comparative analysis of 8-oxo-2′-deoxyguanosine in DNA by ^{32}P-postlabeling and electrochemical detection. *Carcinogenesis 18*, 2367–2371.

(27) Bolton, J. L., Trush, M. A., Penning, T. M., Dryhurst, G., and Monks, T. J. (2000) Role of quinones in toxicology. *Chem. Res. Toxicol. 13*, 135–160.

(28) Han, X., and Liehr, J. G. (1994) 8-Hydroxylation of guanine bases in kidney and liver DNA of hamsters treated with estradiol: Role of free radicals in estrogen-induced carcinogenesis. *Cancer Res. 54*, 5515–5517.

TX700428M

Arch Environ Contam Toxicol (2008) 55:199–209
DOI 10.1007/s00244-007-9110-5

Aryl Hydrocarbon Receptor and Estrogen Receptor Ligand Activity of Organic Extracts from Road Dust and Diesel Exhaust Particulates

Kentaro Misaki · Masato Suzuki · Masafumi Nakamura · Hiroshi Handa · Mitsuru Iida · Teruhisa Kato · Saburo Matsui · Tomonari Matsuda

Received: 8 August 2007 / Accepted: 3 December 2007 / Published online: 8 January 2008

Abstract A wide variety of contaminants derived from diesel and gasoline engines, tire, asphalt, and natural organic compounds is found in road dust. Polycyclic aromatic compounds (PACs) are the important toxic targets among various contents in road dust and diesel exhaust particulates (DEPs), and endocrine-disrupting activity of PACs was suggested. In the present study, aryl hydrocarbon receptor (AhR) ligand activity was confirmed in the extract of both road dust and DEPs. In the separation of the extracts for both road dust and DEPs with reversed-phase HPLC, it was found that polar fractions contributed to significant AhR ligand activity in both a mouse hepatoma (H1L1) cell system and a yeast system. Furthermore, the contribution of these polar fractions was higher in DEPs than in road dust, probably because of the greater concentration of oxy-PAHs in DEPs than in road dust. The contribution of contaminants associated with the polar region to AhR ligand activity was also evident following the separation of road dust with normal-phase HPLC. Additionally, remarkable estrogen receptor (ER) ligand activity was detected in the highly polar region separated with normal-phase HPLC. It is suggested that many unknown AhR or ER ligand active compounds are contained in the polar region.

K. Misaki · M. Suzuki
Department of Environmental Engineering, Graduate School of Engineering, Kyoto University, Yoshida-honmachi, Sakyo-ku, Kyoto 606-8501, Japan

K. Misaki · S. Matsui · T. Matsuda (✉)
Department of Technology and Ecology, Graduate School of Global Environmental Studies, Kyoto University, Yoshida-honmachi, Sakyo-ku, Kyoto 606-8501, Japan
e-mail: matsuda@z05.mbox.media.kyoto-u.ac.jp

M. Nakamura · H. Handa
Hiyoshi Corporation, 908 Kitanosho-cho, Omihachiman, Shiga 523-8555, Japan

M. Iida · T. Kato
Otsuka Pharmaceutical Company, Ltd, 224-18 Ebisuno Hiraishi, Kawauchi-cho, Tokushima 771-0195, Japan

Road dust is an important nonpoint pollution source because it is transported through storm water runoff, which is generally discharged into aquatic environments without treatment (Lee et al. 2005a, b). Road dust includes various metals and inorganic and organic compounds derived from diesel and gasoline engines (Rogge et al. 1993b; Crepineau et al. 2003).

To the surface of the carbon core in diesel exhaust particulates (DEPs), various contaminants are adhered. These contaminants include organic substances, metals (Fe, Cu, Co, V, etc.), and sulfates, nitrates, and ammonium salts of these acids (Mcdonald et al. 2004). The main organic compounds included in an extraction solution of DEPs with organic solvent are aliphatic compounds (aliphatic hydrocarbons and aliphatic acids), polycyclic aromatic compounds (PACs), steranes and hopanes derived from natural compounds, phthalic acid esters, etc. PACs include polycyclic aromatic hydrocarbons (PAHs), oxygenated PAHs (oxy-PAHs; polycyclic aromatic ketones [PAKs], polycyclic aromatic quinones [PAQs], hydroxylated PAHs [hydroxy-PAHs], polycyclic aromatic carboxaldehydes, polycyclic aromatic carboxylic acids, polycyclic aromatic lactones, polycyclic aromatic anhydrides), and nitrogenated aromatic compounds such as nitro-PACs and heterocyclic amines (Rogge et al. 1993a; Alsberg et al. 1985; Casellas et al. 1995; Hannigan et al. 1998; Pedersen et al. 2005; Fernandez et al. 1992; Kannan et al. 2000). Besides contents derived from diesel and

gasoline engines, road dust is also thought to include natural resins, polyethylene glycol ethers, and high-ring-number PACs derived from tires and asphalt, and natural organic compounds transferred from airborne particulates, etc., are also thought to be included (Rogge et al. 1993b).

PACs are important toxic targets among various contents in road dust and DEPs and accumulate in the sediment of aquatic environments via storm water runoff (Kannan et al. 2000; Fernandez et al. 1992), and some wildlife and humans have the risk of exposure to them. Many studies of PAC mutagenicity and carcinogenicity have been reported (Durant et al. 1996; Machala et al. 2001a; IARC 1983), however, studies on endocrine-disrupting activity of PACs are few.

Since the 1990s, the importance of endocrine-disrupting activity of environmental contaminants has been emphasized (Colborn et al. 2004; Vos et al. 2000). Endocrine-disrupting phenomena by diesel exhaust have often been reported for male mice and rats (Yoshida et al. 2000; Tsukue et al. 2001, 2004; Watanabe et al. 1999; Wells et al. 1997; Matsumoto et al. 1986), and diesel exhaust has been connected primarily with antiandrogenic and estrogenic activity (Okamura et al. 2004; Kizu et al. 2003; Ohtake et al. 2003; Machala et al. 2001b). It was also reported that the mass of storage tissue and production of gametes decreased in marine mollusks exposed to diesel oil (Moore et al. 1989). These endocrine disruption activities of diesel exhaust and oil are likely to be caused by PACs such as benzo[*a*]pyrene (B[a]P), however it has not yet been determined what compounds contribute most to this activity (Okamura et al. 2004; Kizu et al. 2003; Ohtake et al. 2003, 2007; Machala et al. 2001b). Some PACs and hydroxy-PAHs showed estrogenic ligand activity for culture cells via direct binding to the estrogen receptor (ER) (Machala et al. 2001b; Clemons et al. 1998; Kamiya et al. 2005; Hirose et al. 2001; van Lipzig et al. 2007). It is also supposed that PACs cause endocrine disruption via the aryl hydrocarbon receptor (AhR) and that the induction of enzymes such as CYP1A1 mediated by AhR is likely to be one of the biomarkers for endocrine disruption (Okamura et al. 2004; Kizu et al. 2003; Ohtake et al. 2003, 2007; Machala et al. 2001b). The association between AhR ligand activity and the inhibition of androgen receptor (AR) response gene expression has been reported (Okamura et al. 2004; Kizu et al. 2003). The pathway via ER-AhR binding interaction has also been predicted for endocrine-disrupting activity in male reproductive organs under PAC exposure (Ohtake et al. 2003). Moreover, the phenomenom that degradation of hormone receptors (e. g., ER and AR) can be mediated by the AhR ligand-dependent ubiquitin-proteosome system (Ohtake et al. 2007) has also been reported.

A ligand activates AhR and AhR transfers into the nucleus and forms the AhR complex by binding with the AhR nuclear translocator. The AhR complex binds xenobiotic response elements and mediates the expression regulation of gene expression, including specific CYPs, glutathione-*S*-transferases, NAD(P)H-dependent quinone oxidoreductase 1, growth factors, and cytokines (Schmidt et al. 1996; Giesy et al. 2002). Many environmental pollutants or natural substances (dioxins, PAHs, tryptophan derivatives, etc.) bind and activate the AhR as exogeneous or endogeneous ligands (Miller et al. 1999; Ziccardi et al. 2002; Clemons et al. 1998; Machala et al. 2001a, b; Till et al. 1999; Jones et al. 1999; Okamura et al. 2004; Bols et al. 1999; Chou et al. 2006, 2007; Denison et al. 2002; Adachi et al. 2001). In our previous study, the AhR ligand activity of oxy-PAHs, such as PAKs and PAQs more polar than PAHs, and the contribution of these polar compounds to the AhR ligand activity of atmospheric samples were reported (Misaki et al. 2007a, b; Machala et al. 2001b).

It is significant to grasp the generous distribution of PAC contents and the hormone receptor ligand activity depending on chemical properties such as polarity in fractions separated using HPLC, from road dust and DEP extracts, for the purpose of toxicological quality control corresponding to compound groups in storm water runoff as a nonpoint source of aquatic environments (Lee et al. 2005a–c; Kawanishi et al. 2004). However, the overvall distribution is unknown in detail (Clemons et al. 1998). In the present study, separation of extracts of both road dust and DEPs was performed with reversed-phase HPLC, and AhR ligand activity for these fractions was measured. AhR ligand activity was evaluated with both luciferase activity in mouse hepatoma (H1L1) cells (chemical activated luciferase gene expression [CALUX] assay) (Ziccardi et al. 2002; Denison et al. 1998) and β-galactosidase activity from a reporter plasmid in yeast, engineered to express human AhR and AhR nuclear translocator proteins (Miller et al. 1999). Additionally, AhR and ER ligand activity was investigated for fractions of road dust separated with the combination of three kinds of columns (Sephadex and normal- and reversed-phase columns). ER ligand activity was evaluated using Chinese hamster ovary (CHO-K1) cells transfected with the human ER gene (Iida et al. 2003; Kojima et al. 2003; Kitamura et al. 2005).

Materials and Methods

Chemicals

DMSO, methanol, acetonitrile, hexane, and chloroform, HPLC grade, were purchased from Wako Chemical (Osaka, Japan). Most PACs were supplied by Sigma-Aldrich Co. (St. Louis, MO, USA). The other PACs were supplied by Nacalai Tesque Co. (Tokyo), Wako Chemical, Tokyo Kasei Co. (Tokyo), and Promochem (Wesel,

Germany). The purity of many PACs was 99%–100%. The purities of benzo[*b*]fluoranthene, benzo[*k*]fluoranthene, anthraquinone, 7,12-benz[*a*]anthracenequinone, and *β*-naphthoflavone (*β*-NF) were 98%. The purities of triphenylene, dibenz[*a*,*h*]anthracene, phenalenone, and 5,12-naphthacenequinone were 97%.

11*H*-Benzo[*a*]fluoren-11-one, 11*H*-benzo[*b*]fluoren-11-one, and 6*H*-benzo[*c*,*d*]pyren-6-one were synthesized as described previously (Misaki et al. 2007). These compounds were purified by column chromatography and recrystallization. The purities of these three synthesized compounds were >99% as judged by HPLC.

Sampling and Extraction

Road dust was collected from Meishin Expressway (Yokaichi IC–Ryuoh IC–Ritto IC) in an urban area of the southern part of Lake Biwa, Japan, at September 28, 2001. The traffic density between 7 AM and 7 PM on October 7, 1999, was 38,598 vehicles/12 h at the sampling site between Yokaichi IC and Ryuoh IC and 46,974 vehicles/12 h at the sampling site between Ryuoh IC and Ritto IC. Road dust was collected and transported to the laboratory as described previously (Lee et al. 2005b). After air-drying in the dark, 5 kg of the sample was sieved through a 500-μm stainless-steel sieve (JISZ 8801, Iida, Japan) to remove gravel, leaf material, glass, and other debris, then ~700 g of sieved sample was separated. Extraction of organic contents from the sieved sample was done using an accelerated solvent extractor (ASE-200; Dionex). The sieved sample (5 g) with 40 g of glass beads was placed in each extraction cell of the ASE. Extraction was carried out twice with dichloromethane under conditions of 100 atm, 100°C for 5 min, static time of 5 min, purge time of 90 s, and flush of 60%. The extraction solution was evaporated using a rotary vaccum evaporator, and 13.5 g of extract was obtained.

DEPs were obtained from an Isuzu Model A4JB1 engine (2740 cm^3, 4-cylinder direct injection type) running on a chassis dynamometer under loads of 30% (torque, 10 kg-m; 1500 rpm) of a maximum engine load fixed at 2000 rpm (Okamura et al. 2004). Exhaust gas containing particulate matter was diluted with clean air in a dilution tunnel, and the DEPs accumulated in the tunnel were collected. Twenty milligrams of DEPs was ultrasonically extracted with 160 ml of chloroform for 10 min and the solution was evaporated to dryness in vacuo.

Separation of Sample Extracts

An extract sample of road dust, 5 mg, was dissolved in 200 μl of DMSO (3% $CHCl_3$) and filtered with a 0.2-μm polytetrafluoroethylene (PTFE) filter (liquid chromatography 13CR; Pall Co., East Hills, NY, USA). Fifty microliters of filtered solution was injected into an analytical HPLC column (Shimpack FC-ODS; ø4.6 × 150 mm; Shimadzu, Kyoto, Japan). An extract sample of DEPs, 5 mg, was dissolved in 200 μl of DMSO (3% $CHCl_3$) and filtered with a 0.2-μm PTFE filter. Fifty microliters of 10 × diluted solution of the filtrated solution with DMSO was used for injection.

Separation Conditions Using HPLC

The separation of injected solution, 50 μl (equivalent to ~1 mg of road dust extract and ~100 μg of DEP extract), using a reversed-phase analytical HPLC column, was eluted with water-acetonitrile as the mobile phase (a linear gradient of water containing 20%–100% acetonitrile for 0–20 min and 100% acetonitrile for 20–80 min) over 80 min at a flow rate of 1.0 ml/min. A fraction was collected every 1 min, evaporated, and dissolved in 20 μl of DMSO. The fraction solution from the road dust extract was subjected intact to yeast and CALUX assay, and the fraction solution from the DEP extract was subjected intact to yeast and as a 10 × diluted solution to CALUX assay. The reversed-phase HPLC system constituted an LC-10ATvp pump, a SIL-10ADvp UV-VIS detector at 254 nm, an SCL-10Avp system controller (Shimadzu), and a fraction collector (SF-2120; Advantec, Tokyo). AhR ligand activity is expressed as *β*-NF equivalent concentration. The *β*-NF equivalent concentration (as a quantitative index) to express observed AhR ligand activity was defined as the *β*-NF concentration at which the activity value was the same as the value for each fraction.

Extract of road dust, 20 mg, was dissolved in 1 ml of mixture solvent of hexane-chloroform-methanol (1:1:1). The solution was injected to a Sephadex HPLC column (Sephadex LH-20; ø10 × 250 mm; GL Sciences Inc., Tokyo) and eluted with hexane-chloroform-methanol (1:1:1) as the mobile phase (isocratic) over 40 min at a flow rate of 2.5 ml/min. Four hundred microliters of the fraction solution (2.5 ml) collected every 1 min was evaporated and dissolved in 20 μl of DMSO. This solution was subjected intact to AhR assay with yeast and ER assay. This separation was repeated and the fractions showing AhR ligand activity (fractions 5–20) were pooled and evaporated. Twenty milligrams of the residue was dissolved in 1 ml of mixture solvent of hexane-chloroform (85:15). Six hundred microliters of the solution (equivalent to 12 mg of the residue) was injected into a normal-phase HPLC column (Wakogel LC30H; ø10 × 250 mm; Wako) and was eluted with hexane-chloroform as the mobile phase (a linear gradient of hexane containing 15%–100% chloroform for

0–30 min and 100% chloroform for 30–100 min) over 100 min at a flow rate of 2.5 ml/min. One hundred microliters of the fraction solution (2.5 ml) collected every 1 min was evaporated and dissolved in 20 μl of DMSO. This solution was subjected intact to AhR assay with yeast and as a 10 × diluted solution to ER assay. The Sephadex and normal-phase HPLC system constituted an LC-10ADvp pump, a SIL-10ADvp UV-VIS detector at 254 nm, an CT-10Avp column oven at 40°C, and an SCL-10Avp system controller (Shimadzu). Two and four-tenths milliliters of the fraction 9 solution was evaporated and the residue was dissolved in 70 μl of DMSO. Fifty microliters of the solution was injected into a reversed-phase HPLC column, and fractionation and AhR assay with yeast were carried out as described above. The UV absorption pattern of these separated fractions showed a similar pattern in at least two handlings.

Yeast Assay

The assay was performed as described previously (Misaki et al. 2007b). *Saccharomyces cerevisiae* strain YCM3 was grown in synthetic glucose medium at 30°C overnight in a shaking incubator (Miller et al. 1999). The next day 10 μl from the saturated culture was inoculated into glass tubes containing 400 μl of a synthetic 2% galactose medium. Each fraction solution dissolved in 2 μl of DMSO was added to the medium to achieve a final solvent concentration of 0.5%, followed by 18 h of incubation at 30°C. The yeast exposed to each fraction solution was incubated in a 96-well plate at half-volume scale in glass tubes, for the experiments combining three kinds of columns. Cell densities were determined by reading the absorbance at 595 nm, and 10 μl of the cell suspension was added to 140 μl of Z-buffer (60 mM Na_2HPO_4, 40 mM NaH_2PO_4, 1 mM $MgCl_2$, 10 mM KCl, 2 mM dithiothreitol, and 0.2% Sarkosyl). The reaction was started by adding 50 μl of *o*-nitrophenyl-β-D-galactopyranoside (ONPG; 4 mg/ml solution in Z-buffer). Samples were incubated at 37°C for 60 min. Absorbances of the reaction mixture were read in a spectrophotometer at 405 nm. The activity of β-galactosidase (referred to as lacZ units) was calculated by the following formula: $412 \times A_{405\ nm}/(400 \times A_{595\ nm} \times$ ml of cell suspension added × minutes of reaction time). The activity is also expressed as β-NF equivalent concentration (Adachi et al. 2001; Chou et al. 2006, 2007). The β-NF equivalent concentration was defined as the β-NF concentration at which the activity value was the same as the value for each fraction. The β-NF equivalent concentration was calculated from the dose-response curve of β-NF (as a positive standard). The results of yeast assay of these separated fractions showed a similar pattern in at least two experiments.

CALUX Assay

The assay was also performed as described previously (Misaki et al. 2007b). Mouse hepatoma (H1L1.1c2) cells ($\sim 1.5 \times 10^5$ cells/well) were cultured in 96-well culture plates, and each fraction solution dissolved in DMSO was added to the medium to achieve a final solvent concentration of 1% (Ziccardi et al. 2002; Denison et al. 1998). After the plates were incubated at 37°C in 5% CO_2 for 24 h, the cell viability was confirmed under a microscope. Subsequently, the medium was removed and the cells were lysed with 30 μl of lysis buffer. Fifty microliters of luciferin (firefly) solution was added to all assay wells according to protocol (Luciferase Assay System, Promega Co., Madison, WI, USA), then immediately luciferase activity was determined under a Lucy1 luminometer (Anthos Co., Eugendorf, Austria) and is reported as relative light units (RLUs). CALUX assay was done one time.

ER Ligand Activity Assay

ER ligand activity assay was performed as described in previous studies with some modifications (Iida et al. 2003; Kojima et al. 2003; Kitamura et al. 2005). Chinese hamster ovary (CHO-K1) cells (8400 cells/well) were plated in 96-well plates at 84 μl/well at a density of 1×10^5 cells/ml in phenol red-free DMEM/F12 medium supplemented with 5% charcoal dextran-treated FBS. CHO cells were cultured for 24 h at 37°C, under 5% CO_2 (Iida et al. 2003; Kojima et al. 2003; Kitamura et al. 2005). Each fraction of DMSO solution was diluted 12.5 times with DMEM/F12 with no supplement, so that the final DMSO concentration was 0.08% (v/v). We transfected cells with 6.25 ng pcDNAERα or pcDNAERβ, 62.5 ng pGL3-tkERE, and 10 ng pcDNA-enhanced green fluorescent protein (EGFP) at 6 μl/well using the transfection reagent FuGene6 (Roche Diagnostics Co., Indianapolis, IN, USA). After a 3-h transfection period, cells were dosed with 10 μl of each diluted fraction solution and cultured for 24 h. The solvent control and 1 nM estradiol (final concentration), which served as the positive control, were incubated in each plate. Following 24 h of culture, green fluorescence radiating from living cells was measured prior to luminescence measurement with a Wallac 1420 ARVO SX multilabel counter (Perkin-Elmer, Boston, MA, USA). Then the luciferase substrate with cell lysis reagent Steady-Glo (Promega Co.) was added to all assay wells in the same plate. The plate was shaken at room temperature for 5 min, then the luciferase activity was determined under a luminometer and is reported as relative light units (RLUs). The results of ER ligand activity assay for these separated fractions showed a similar pattern in at least two experiments.